Lecture Notes for:
ACCELERATOR PHYSICS AND TECHNOLOGIES FOR LINEAR COLLIDERS

Physics 575
University of Chicago
January 22nd and 24th, 2002

Tor Raubenheimer
Stanford Linear Accelerator Center
Stanford University

Contents

1. IP Issues and Luminosity

The two primary parameters for a linear collider are the center-of-mass (cms) energy and the luminosity. The luminosity, multiplied by the cross-section of interest, gives the event rate:

$$L = \frac{f_{rep} n_b}{2p} \frac{N_+ N_-}{\Sigma_x \Sigma_y} H_D$$

Where n_b is the number of bunches per rf pulse, f_rep is the pulse repetition rate, N are the number of particles per colliding beam, and Σ are the horizontal and vertical sizes of the two colliding beams summed in quadrature:

$$\Sigma^2 = s_+^2 + s_-^2$$

Finally, H_D is the luminosity enhancement that arises from the attraction of the two beams.

In a linear collider, the pulsed repetition rate tends to be low f<200 Hz because of limits on the pulsed rf systems and energy efficiency issues. Fortunately, there is only a weak beam-beam limit and so the luminosity is attained through very small spot sizes. However, small spot sizes require strong focusing at the IP and very small transverse emittances – the emittance is the beam phase space area.

Luminosity and beam parameters in rings vs. linear colliders

	Lum.	**f_rep**	**n_b**	**N [10^{10}]**	**sx [mm]**	**sy [mm]**
NLC	10^{34}	120 Hz	192	0.75	0.250	0.003
SLC	$2x10^{30}$	120 Hz	1	4	1.5	0.7
LEP2	$5x10^{31}$	10 kHz	8	30	240	4
PEP-II	$3x10^{33}$	140 kHz	1700	4	155	6

IP Issues:

- Disruption (Δν, beam-beam deflections)
- Pinch and luminosity enhancement, H_D
- Beamstrahlung and luminosity spectrum
- E+/e- pairs
- Single bunch kink instability
- Crossing angle issues

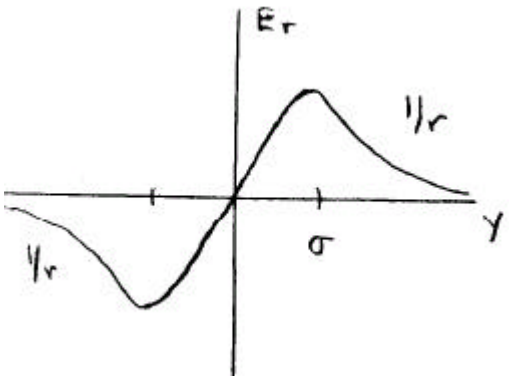

Disruption:

The electric and magnetic space charge forces cancel as $1/\gamma^{**}2$ but during the collision the forces from the opposing bunch add and can have a huge effect. The two beams will focus each other, assuming oppositely charged beams, with a highly nonlinear force. In a storage ring, the beams must continue to circulate and thus the beam-beam force must be kept small. The limits are entirely different in a linear collider.

The beam-beam force can be parameterized with the disruption which is the ratio of the focusing focal length (treating the beam like a thin lense) to the bunch length:

$$D_{x,y} = \frac{2Nr_e}{g}\frac{s_z}{s_{x,y}(s_x + s_y)}$$

The equation of motion for a particle close to the core of an oppositely charged beam where the forces are linear in a beam with a gaussian longitudinal profile is:

$$x'' + x\frac{D_x}{\sqrt{2p}\,s_z^2}e^{-z^2/2s_z^2} = 0$$

and the number of oscillations that particles perform in the opposing bunch is approximately 1.3 sqrt(D)/2π for D>>1.

The disruption causes an increase in the outgoing particle distributions, the beam-beam deflections, the single bunch kink instability, and the pinch effect, which leads to the luminosity enhancement.

Outgoing distributions:

The outgoing particle distributions of the primary beam will be enlarged. The typical angles of the outgoing beam will be set by: $q_0 = \frac{D_y s_y}{s_z} = \frac{D_x s_x}{s_z}$.

Pinch effect and Luminosity Enhancement:

The strong focusing effect between the beams will lead to a dynamic focusing of the opposing beams. This decreases the effective size of the colliding beams and results in an increase in the luminosity, referred to as the luminosity enhancement. In round beams, the luminosity enhancement can be quite large, $H_D >> 1$ however with flat beams where the horizontal beam size is many times the vertical beams size, the enhancement is typically between 1.3 and 2.

An approximate expression that has been found by P. Chen and K. Yokoya for electron-positron collisions where they fit the results of computer simulations:

$$H_D(round) \approx 1 + D_y^{1/4}\left(\frac{D_y^3}{1+D_y^3}\right)\left[\ln\left(\sqrt{D_y}+1\right)+2\ln\left(\frac{0.8}{A_y}\right)\right]$$

where the effective horizontal and vertical spot sizes at collision are: σ_effective ~ σ / sqrt(H_D) and Ay = σz / βy parameterizes the hourglass effect which the depth of focus is smaller than the bunch length and thus the beam size varies during the collision.

In flat beam collisions, with σx >> σy, an approximate form can be written:

$$H_D(flat) \approx \left(H_D(round)\right)^{1/3}$$

and the effective spot sizes are σx_effective ~ σx and σy_effective ~ σy / (H_D)**(1/3). These expressions are valid for A<1 and D<20. The difference between the round and flat cases arises because only the vertical beam size is reduced in the flat beam case and thus neither the luminosity nor the beam-beam forces increase as rapidly.

For electron-electron collisions, the beam-beam forces act to push the beams apart and increase the beam sizes. In these cases, it seems that, after optimization of the parameters, the luminosity enhancement will be in the range of 0.3 ~ 0.1.

In gamma-gamma collisions, the photon beams are generated by colliding polarized electron beams with laser beams at a collision point a few mm before the IP. In this case, the parameters can be optimized to attain similar luminosity enhancements as the electron-electron case for the photon collisions.

Beamstrahlung and luminosity spectrum

As the beam-beam forces focuses the opposing beam and particles are deflected, they can also emit synchrotron radiation which is referred to as beamstrahlung. Note that the incoherent collisions between particles also cause emission of radiation like bremstrahlung which is referred to as the initial state radiation. The photons from the beamstrahlung can be very high energy. These will significantly degrade the luminosity spectrum, make the transport of the disrupted beam much more difficult, and generate backgrounds such as electron-positron pairs and hadronic jets. Finally, the beamstrahlung, which can have MWs

of power, has to be absorbed along with the disrupted beam. For these reasons, the parameters are usually chosen to minimize the beamstrahlung.

There are three parameters, in addition to the disruption parameter, which are useful to describe the beam fields and the beamstrahlung and electron/positron pairs: Y which is the ratio of the classical characteristic photon energy to the beam energy, n_γ which is the average number of beamstrahlung photons emitted, and d_B which is the average energy lost per beam particle due to the beamstrahlung. These can be written:

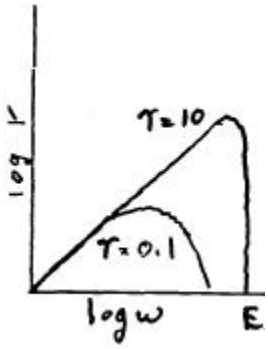

$$Y \equiv \frac{2}{3}\frac{\hbar w_c}{E} \approx \frac{5}{6}\frac{N r_e^2 g}{a s_z (s_x + s_y)} \qquad n_g \approx \frac{2 N r_e a}{s_x + s_y}\frac{1}{\sqrt{1+Y^{2/3}}}$$

$$d_B \approx \frac{5}{4}\frac{a s_z Y^2}{l_e g}\frac{1}{\left(1+(1.5Y)^{2/3}\right)^2}$$

The primary approach to limiting the beam fields and the beamstrahlung without reducing the luminosity is to operate with very flat beams $\sigma x >> \sigma y$. Flat beams also make use of the natural asymmetry in the damping rings and the final quadrupole focusing – a final doublet instead of a triplet.

Figure 1: Luminosity spectrum for three different cms energies

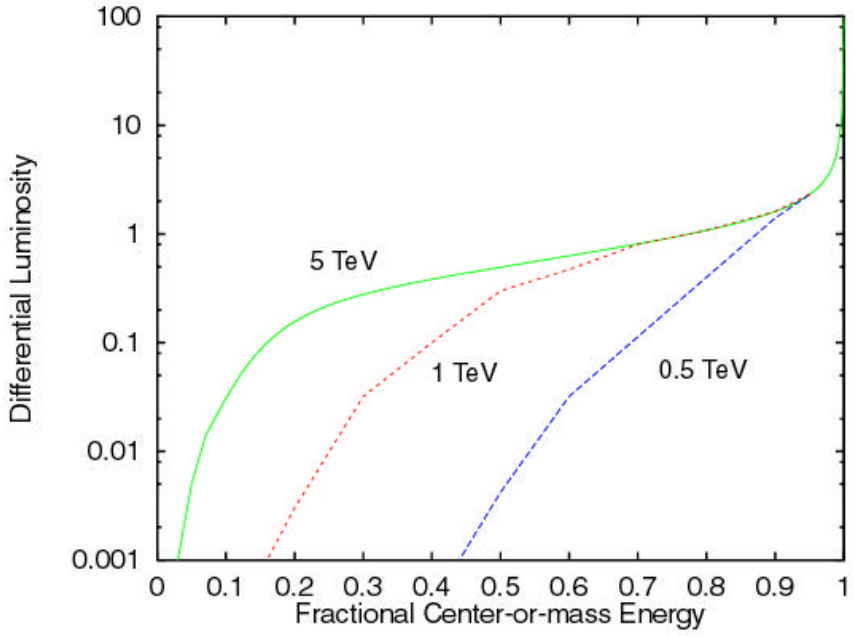

The luminosity spectrum is spread by the beamstrahlung. Although the parameters are strongly coupled, the number of photons is closely related to the luminosity close to the full center-of-mass while the average energy lost describes the tails of the distribution. In particular, the fractional luminosity at the full center-of-mass is given by:

$$L_{100\%} / L_0 = \frac{\left(1 - e^{-n_g}\right)^2}{n_g^2}$$

With flat beams and Y<<1, n_γ primarily depends on the ratio of (N / σx) while d_B depends on (N / σx)**2 and is inversely proportional to the bunch length and proportional to the beam energy. Thus, although n_γ is only weakly dependant on the beam energy, it is very difficult to keep d_B small as the energy is increased. The plot on the previous page shows the evolution of an old CLIC luminosity spectrum as the cms energy was increased.

e+/e- Pairs

E+/e- pairs are a significant background source in the linear colliders. There are two primary sources: incoherent pairs where real and virtual photons scatter off individual particles and coherent pairs where the photons pair-create in the collective beam fields. The later is strongly dependent on Y and only becomes important as Y increases above 0.3 or so. The number of pairs tends to increase exponentially until Y~1 and then starts to slowly decrease again. The figure below is from the NLC Zeroth Order Design Report and shows the number of incoherent and coherent pairs as a function of Y. Unfortunately, Y is also a strong function of the collision energy and it appears that high-energy colliders (E>2 TeV) will have to live with Y >> 1 and the number of coherent pairs becomes comparable to the number of beam particles.

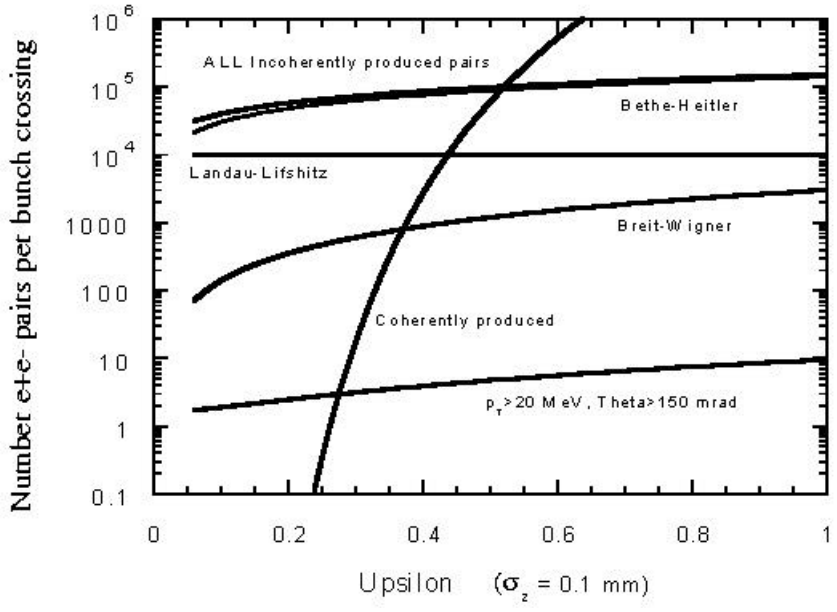

Figure 2: E+/e- pairs vesus Upsilon from NLC ZDR

Beam-beam deflections:

The beam-beam deflection is an essential tool to center the two colliding beams with respect to each other. The beam-beam force will amplify small offsets so that they can be easily measured downstream. For example, in the NLC design, a 0.3 nm (0.1 σy) vertical offset between the colliding beams will cause a 20 μm offset 2 m away from the IP where BPMs could be located. The deflection is roughly equal to the offset in units of the beam size times the angular spread of the outgoing beam θ_0. The effect is reduced at large disruption parameters but is still a very powerful effect.

The beam-beam deflections are also an important diagnostic tool which can be used to calculate the Σx,y of the colliding beams. They were used extensively to tune the SLC IP spot sizes. Here, one of the 'knobs' that controlled the 1st-order aberrations at the IP would be adjusted while performing a beam-beam deflection scan at each point. Typical knobs include the x and y waist location, x ad y vertical dispersion, and x'-y coupling term. An example b-b deflection from the SLC is shown below where a 420 nm vertical beam size was measured.

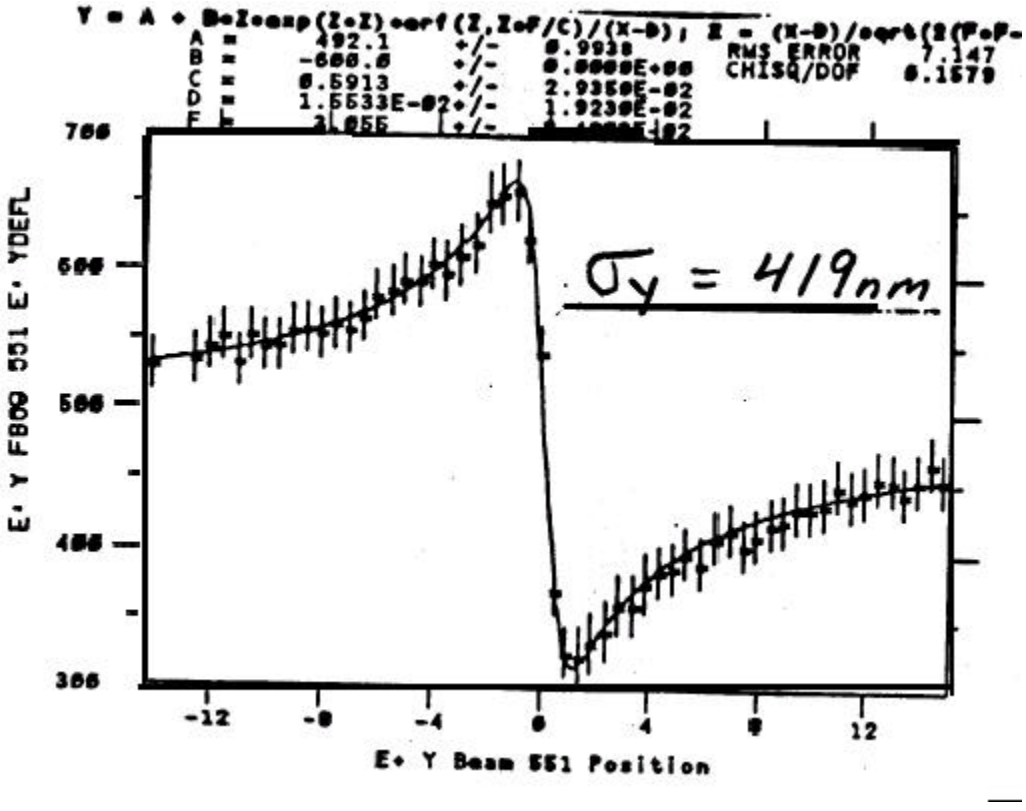

Figure 3: Beam-beam deflection scan from SLC

Unfortunately, it can be difficult to estimate to optimal setting of the aberrations using this technique. During the last SLC run, a dither tuning technique was implemented where the same knobs were tuned against heavily averaged luminosity signals.

Single Bunch Kink Instability:

The single bunch kink instability is a two-stream instability that arises when the disruption parameter becomes very large D >> 10. At low disruption, the attractive force between the two beams will reduce the luminosity reduction to rigid offsets between the beams. However, as the disruption parameter increases, one starts to see large luminosity losses for small offsets. Of course, the greatest sensitivity will occur when the incoming beams are modulated at the oscillation frequency within the opposing beam. Following is a set of three plots showing the sensitivity of the luminosity as a function of the offset amplitude for three different cases: round beams, flat beams with $\beta y >> \sigma z$, and flat beams with $\beta y = \sigma z$ from K. Yokoya, "BEAM-BEAM PHENOMENA IN LINEAR COLLIDERS," Lecture at 1990 US-CERN School on Particle Accelerators, Hilton Head Isl., So. Carolina, Nov 7-14, 1990.

As stated the single bunch kink is a function of the disruption parameter and the modulation wavelength along the bunch. The variation of the position along the bunch can arise from dispersive errors and transverse wakefield effects which dilute the transverse emittance. The effect is worst when the bunch position is modulated at the oscillation frequency within the opposing bunch.

The effect can be quite dramatice – a simulation movie by Andrei Seryi can be found at: http://www.slac.stanford.edu/~seryi/bbeam/.

Figure 4 by Daniel Schulte is a preliminary calculation showing the luminosity loss as a function of the disruption for three different offset values: Δ=0.1, 0.3, and 0.5 σy. In all cases, the geometric luminosity is the same however the beam-beam force is allowed to increase to represent increasing disruption. As the disruption values are increased, the pinch effect leads to a larger initial luminosity value but it also leads to a much greater sensitivity to correlations along the bunch.

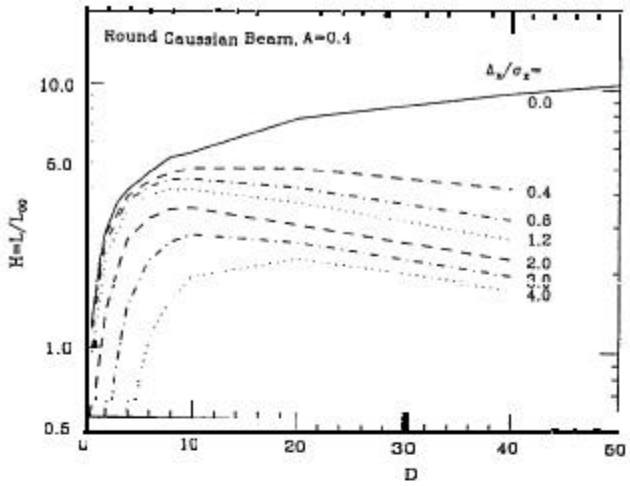

Luminosity for different rigid offsets Δ for a round beam. Note that with round beams the total luminosity enhancement can be >>1

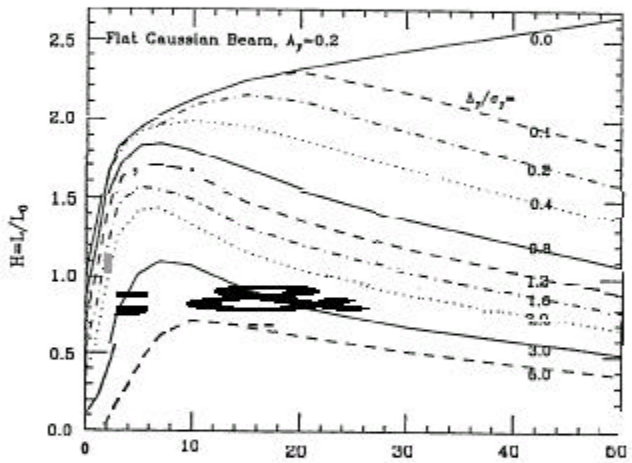

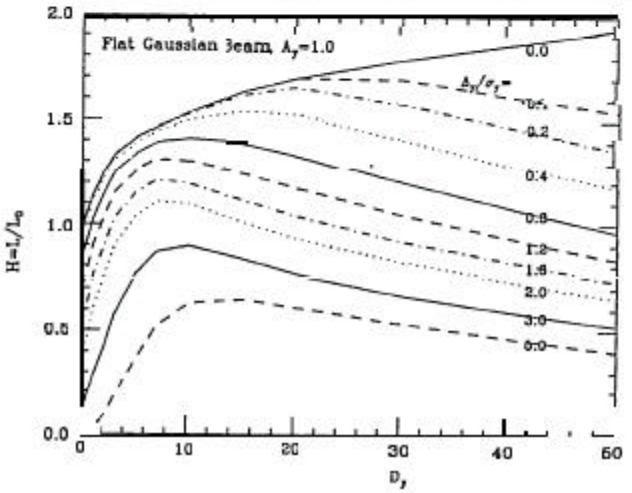

Luminosity for different rigid offsets Δ for a flat beam. The upper plot is with βy << σz and the lower has βy = σz. In both cases, the luminosity enhancement is 1.5~2. Note that for Dy<10, the larger disruption reduces the luminosity loss due to a rigid offset however for larger Dy, the kink instability starts become important.

In practice, this effect may limit the maximum disruption parameter. One approach to comparing different design is to simply use the geometric luminosity and to set effective the luminosity enhancement to 1. The following table lists the IP parameters for NLC, TESLA, and CLIC. Parameters are listed for both the fully diluted beam parameters and the damping ring emittances – the former should be used to estimate the luminosity but the later might be the more appropriate when estimating the disruption parameters and the beam-beam effects.

Figure 4: Preliminary calculation of luminosity loss due to single bunch kink instability by D. Schulte. Luminosity is plotted against the sz/l of an initial sinusoidal modulation of the beam for different disruption parameters.

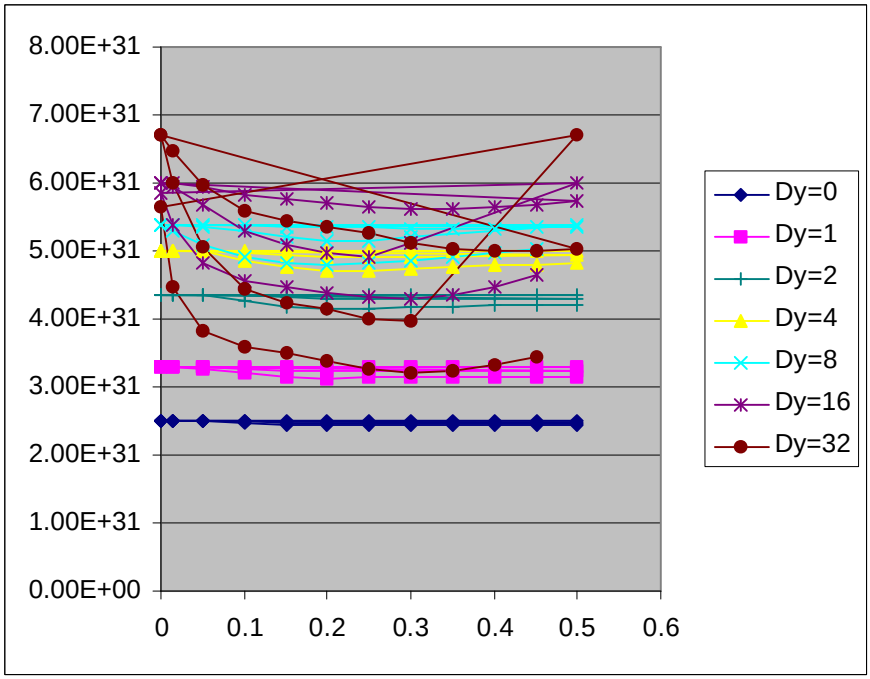

	TESLA		NLC		CLIC
Energy	500		500		3000
N	2.00E+10		7.50E+09		4.00E+09
DR emitx	8.00E-06		3.00E-06		
DR emity	2.00E-08		2.00E-08		
IP emitx	1.00E-05		3.60E-06		6.80E-07
IP emity	3.00E-08		3.50E-08		2.00E-08
betax	15		10		8
betay	0.4		0.1		0.15
sigmax	5.54E-07	4.95E-07	2.71E-07	2.48E-07	4.30E-08
sigmay	4.95E-09	4.04E-09	2.67E-09	2.02E-09	1.01E-09
sigmaz	3.00E-04		1.10E-04		3.00E-05
Dy	**24.82**	**34.02**	**12.89**	**18.71**	**5.14**
L0	1.64E+34	2.24E+34	1.41E+34	2.04E+34	6.67E+34
Approx Hd	2.10E+00	1.81E+00	1.39E+00	1.47E+00	1.91E+00
Approx Lum	3.44E+34	4.06E+34	1.95E+34	2.99E+34	1.27E+35

Table 1: IP parameters for TESLA, NLC, and CLIC

Crab Crossing and Multibunch kink

All of the linear collider designs accelerate long trains of bunches on each rf pulse to be able to obtain the desired luminosity with a 'reasonable' wall plug power. Each rf pulse in TESLA consists of 2820 bunches while each rf pulse in NLC has 192 bunches. As will be discussed, normal conducting accelerators only accelerate efficiently when the average current is relatively high and thus the bunches must be closely spaced – 1.4 ns in the NLC design.

To avoid parasitic collisions, the normal conducting designs must collide the beams at a small angle and a multibunch kink instability. For the next-generation colliders with $Y << 1$, the multibunch kink instability sets a limit of a few mrad. In the 3 TeV CLIC design, where $Y \sim 10$, the e+/e- pairs enhance the kink instability and the minimum crossing angle is closer to 20 mrad.

The superconducting design is different because the beams are separated by roughly 100 m. This allows for head-on collisions where the disrupted beam is deflected from the incoming beam trajectory using electrostatic separators and a septum. Of course, the superconducting design can also use a crossing angle if desired.

A crossing angle with the separate incoming and outgoing beam line can also simplify the outgoing beam line design. In this case, the incoming beam line does not have to absorb the beamstrahlung power which can be on the order of 1 MW and the beam separation, which can be tricky because of the large energy spread in the disrupted beam, is trivial.

If the angle between the two incoming beams is less than $\sigma x/\sigma z$, then there will be minimal luminosity loss from the collision angle. However, this angle is the order of 2 mrad in the NLC design which is too small to separate the beams in the final doublet. The NLC IR layout is shown on the next page with the incoming beamline at positive x and the outgoing beamline at negative x.

To avoid the luminosity loss due to the crossing angle, the beams can be 'crabbed' so that they collide head-on even though they are moving at an angle with respect to each other. The crabbing can either be generated by adding dispersion at the IP so that the energy correlation along the bunch with cause a position offset along the length or with an rf cavity operating in a transverse mode as illustrated on the following page.

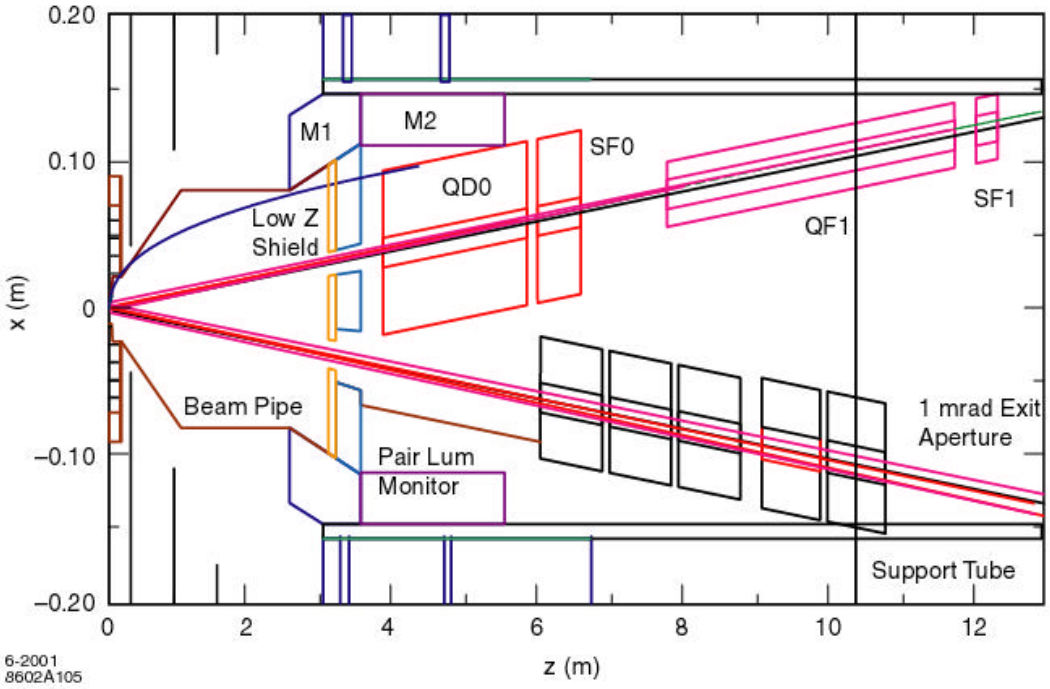

Figure 5: NLC IR layout with 20 mrad crossing angle

The two disadvantages of the crossing angle are: (1) the beam passed through the detector solenoid at an angle causing a vertical deflection at the IP which must be removed by steering the beam and (2) the tolerance on the relative phase of the two crab cavities is tight (~0.05° at S-band for NLC).

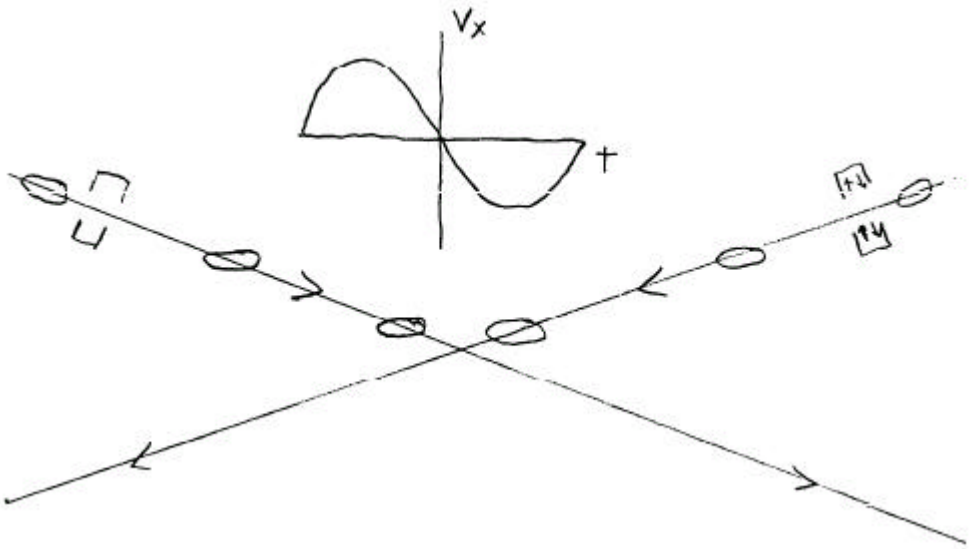

Figure 6: Schematic of crab crossing.

2. Beam Parameters

Luminosity:

In a linear collider, luminosity can be expressed as:

$$L = \frac{P_{beam}}{4pE_{cms}} \frac{N}{s_x} \frac{H_D}{s_y}$$

where P_{beam} is the beam power which is a function of the total ac wall plug power used by the linear accelerator and the efficiency of the rf system in accelerating the beam. Most linear collider designs have ac $\rightarrow$ beam efficiencies that range from 5% to 25%.

Assuming that flat beams are chosen to constrain the beamstrahlung, the luminosity can be rewritten using ? and d_B as:

$$L \propto \frac{P_{beam}}{E_{cms}} \sqrt{\frac{d_B s_z}{ge_y b_y}} H_D \left(1 + (1.5\mathrm{Y})^{2/3}\right)$$

It does not make sense to reduce the vertical beta function much beyond the bunch length because the hourglass effect will reduce the luminosity while the smaller beta function will require tighter tolerances in the final focus.

It is frequently noted that, for small Y, the final term can be dropped and the luminosity is effectively determined by the beam power, the vertical emittance, and the beamstrahlung energy spread. Of course, this is a scaling law and like all scaling laws it is not valid to use for detailed comparisons. Furthermore, for most normal conducting linear collider designs, which operate with Y between 0.1 and 0.3, the final term is important and actual changes the scaling.

A more appropriate expression for the next generation of linear colliders with Y less than 0.3 might be:

$$L \propto \frac{P_{beam}}{E_{cms}} \sqrt{\frac{1}{ge_y b_y}} n_g H_D$$

This expression is more closely related to the quantity that describes the luminosity near the center-of-mass as well as being more accurate over the range. Alternately, the luminosity can be written in terms of the disruption which should not be allowed to become too large or the single bunch kink instability will eliminate any luminosity gains.

Other important constraints on the IP parameters include the final focus limitations, which make very small IP beta functions difficult and final doublet vibration issues, which may limit the final spot size. The Final Focus Test Beam at SLAC focused a large emittance

beam to beta functions of roughly 10 mm x 100 μm. These betas are similar to the goals for the next generation colliders.

Detailed parameter tables can be found at the end of these notes. There are six tables which cover: overall parameters, damping rings, bunch compressors and pre-linacs, main linacs, beam delivery systems, and particle sources. These are draft versions of the tables that are being used by the Technical Review Committee on Linear Colliders, chaired by Greg Loew.

The parameters listed in the tables are a representative set however all the colliders are designed to operate over a wide range of parameters. For example, if a resonance needs to be measured very accurately, the bunch charge could be reduced, reducing the beamstrahlung at the expense of the luminosity. Decreasing the bunch charge and the average beam current will also allow the collider to operate at higher beam energies because the beam loading is reduced. On the other hand, it may be desired to operate with the highest possible luminosity. In this case, the bunch charge could be increased and the bunch separation increased to hold the average current constant. This would nominally double the luminosity, although consideration does need to be given to the single bunch kink and the disruption parameter.

Beam Power and Efficiency:

As seen, the efficiency of the generation and transfer to the beam is an important parameter because the beam power is directly proportional to the luminosity and ac wall plug power is expensive. Given a basic technology, the cavity and beam parameters must be chosen to optimize the transfer of power. This actually is a balance between making the most efficient transfer of energy and maintaining reasonable overhead so that small fluctuations in the beam current do not change the cavity voltages excessively.

The accelerator cavities are described by a Q and a shunt impedance $R = V^2/Pc$ where V is the cavity voltage and Pc is the power lost to the walls. The quantity R/Q is roughly constant for all standard cavities and is ~100 – this is determined by the cavity geometry. There are two types of accelerator structures: standing wave cavities and traveling wave cavities. For efficient operation in a standing wave cavity, the input coupler is matched so that the power flow into the cavity equals that extracted by the beam and lost to the walls. In a traveling wave cavity, the input and output couplers are matched to the cavities as a transmission line.

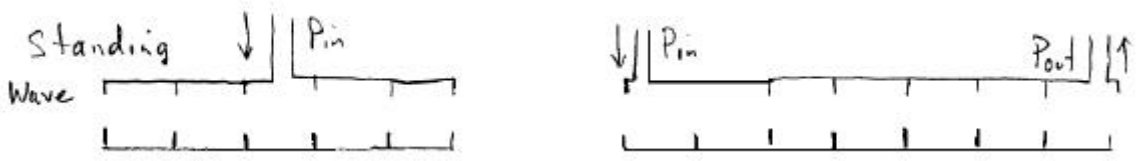

Figure 7: Schematic of standing and travelling wave cavities

In a standing wave cavity, the rf efficiency is simply:

$$h \approx \frac{P_b}{P_c + P_b} \frac{1}{\left(1 + \frac{T_{fill}}{T_{beam}}\right)}$$

where Pb is the instantaneous beam power (the average beam power is related to this by the duty cycle), Pc is the cavity losses, Tfill is the cavity fill time, and Tbeam is the beam pulse length. Thus, the rf efficiency of a superconducting cavity is simply given by the ratio of the beam pulse length to the rf pulse length.

Maximum efficiency is obtained when the voltage induced by the beam is ½ the zero current cavity voltage. The beam current is determined by the cavity voltage and the input power which is limited by the couplers. With an input coupler that can handle 230 kW, the beam current is limited to about 10 mA. In this case, the external Q of the cavity is given by:

$$Q_{ext} \approx Q \frac{V}{I_b R}$$

and the cavity filling time is time which it takes the cavity voltage to reach 50% at which point the beam is injected and this voltage is maintained. Thus, Tfill ~ 0.68 * 2Qext/ω. Finally, the beam time Tbeam is limited by the overall duty cycle which is determined by the average heat load and the instantaneous temperature rise in the cavities. To obtain a good ac-to-beam efficiency, TESLA has chosen a beam time that is roughly 2 times that of the cavity fill time and a repetition rate of 5 Hz. Finally, although the power lost to walls is small in a superconducting cavity, the cryogenic power is roughly 600 times the power lost at 2K and this must be added to the previous results.

In a traveling wave structure, the optimization is slightly different. Here, the fill time of the cavity, i.e. the time for power to pass through the structure, relative to the dissipation time is the relevant quantity:

$$t = \frac{wL}{2Q\overline{v_g}}$$

where L is the structure length and vg is the group velocity of the power through the structure. Normal conducting structures can be nearly as efficient as the superconducting structures however, in this case, they have to be very short so the dissipation into the walls is small. The efficiency is optimal for an infinitely long bunch train when $\tau = 1/J$ where J is the normalized beam current:

$$J = \frac{I_b R}{V_u}$$

where Vu is the unloaded beam voltage. The rf efficiency curves for a constant gradient structure are shown below.

For maximum efficiency, the cavity voltage is half the unloaded voltage as in the superconducting case. In practice, normal conducting accelerators are rarely operated with such a high beam loading. In the NLC case, J is roughly 1.4 and the loaded voltage is about 75% of the unloaded voltage. The τ parameter is chosen to be 0.53 rather than 0.70. In this case, the efficiency is given by:

$$h = 2tg(t)J\left[1-\frac{J}{2}\left(1-\frac{2te^{-2t}}{1-e^{-2t}}\right)\right]\frac{1}{\left(1+\frac{T_{fill}}{T_{beam}}\right)}$$

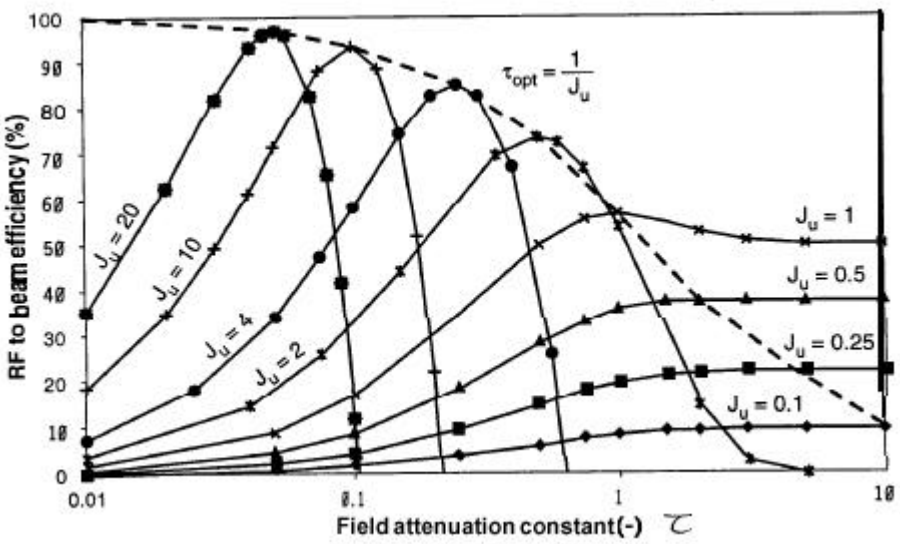

Figure 8: Efficiency curves for a constant gradient travelling wave structure

In the end, the rf-to-beam efficiency for TESLA is about 63% while it is slightly more than half of that for NLC but the power needed for the cryogenics system makes up some of the difference. The power flow for the two machines is illustrated in Fig. 10.

Layout:

These basic issues determine the basic layout of the linear collider facilities:

- Electron and positron sources to generate long bunch trains

- Damping rings to decrease the beam emittance

- Bunch compressors to decrease the damping ring bunch length to something matched to the linac

- Efficient main linacs to accelerate the beam to the desired energy while preserving the beam emittance

- Final focus systems to focus the low emittance beams to the small spots sizes needed at the IP

The NLC and TESLA schematics are shown below illustrating the different sections – none of which are drawn to scale although both facilities are roughly the same overall length. In the following, we will discuss the rf-to-beam efficiency as well as the fundamental differences between the superconducting and normal conducting approaches since these are closely related to total beam power and therefore the luminosity.

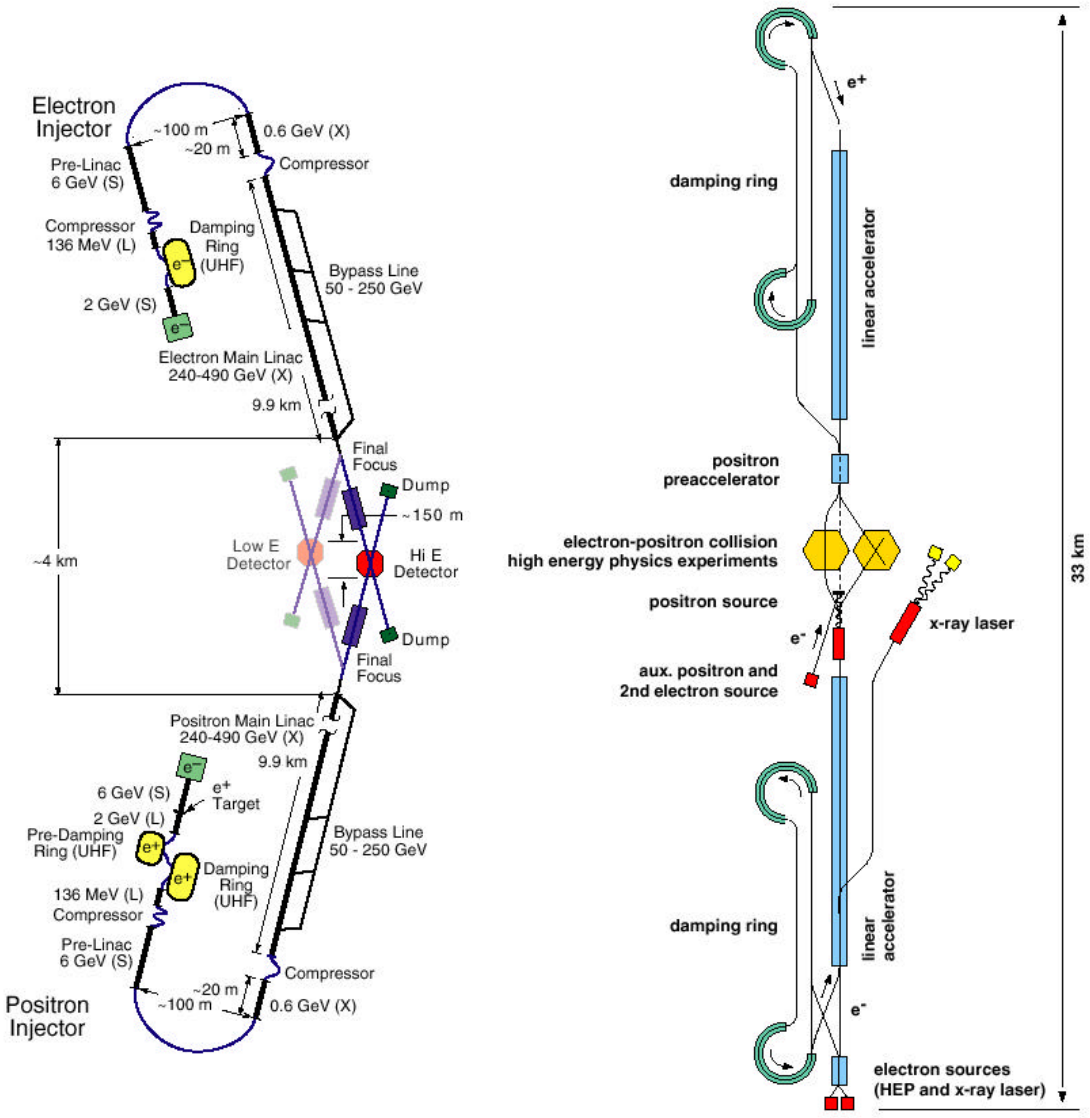

Figure 9: Schematic of NLC and TESLA

3. RF Power Generation

The rf system of a linear collider consist of four sections:

- Modulators which convert line ac to pulsed dc for the klystrons
- Klystrons which convert the pulsed dc to pulsed rf power
- Rf distribution (and compression) which transport the rf to the accelerator structures and may temporally compress the power to increase the amplitude
- Accelerator structures which transfer the rf power to the beam

As discussed, the efficiency of the generation and transfer to the beam is an important parameter because the beam power is directly proportional to the luminosity and ac wall plug power is expensive. A schematic by Chris Adolphsen for the power generation is shown below with efficiencies for NLC and TESLA. All parts of the power system must be optimized for efficiency.

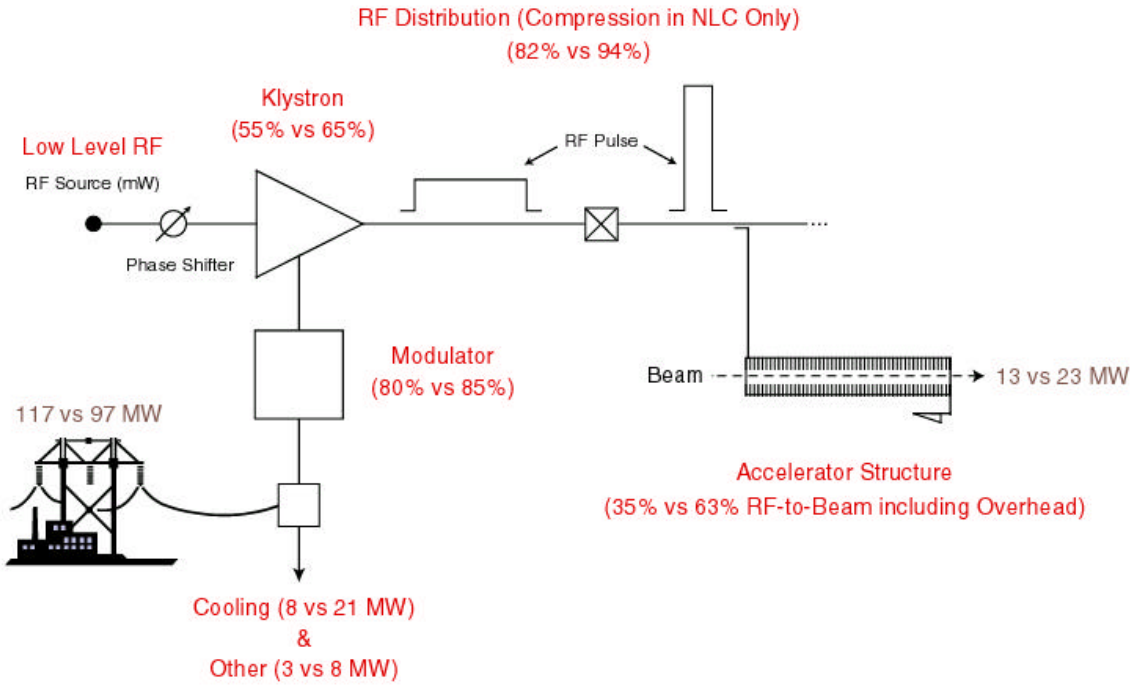

Figure 10: Schematic of power distribution in a linear collider

Modulators:

The modulators must convert the line dc to pulsed ac for the klystrons. The basic system is just a large capacitor and a switch—the capacitor then discharges through the load of the klystrons. The challenging aspects are the voltages and powers involved. The following table lists the TESLA and NLC modulator requirements. To make the system efficient requires minimizing the switching times—this is especially important for the relatively short pulse for the NLC. The solution to this problem is to minimize the inductance.

Table 1: NLC and TESLA Modulator parameters

	NLC	TESLA
Output voltage	500 kV	115 kV
Output current	2120 A	130 A
Repetition rate	120 Hz	5 Hz
Pulse length	3.2 μs	1.4 ms
Rise/fall time	200 ns	200 μs
Energy per pulse	3.4 kJ	21 kJ
Transformer ratio	3:1 step up	12:1 step up
Output load	Eight 75 MW klystrons	One 10 MW klystron
Efficiency	>80%	>85%

At this point in time, both TESLA and NLC are designing modulators based on solid-state switches: Integrated Gate Bipolar Transistors which were developed for the electric train industry. Each of these devices can switch 10's of MWs. The circuit schematic for the NLC design is shown below.

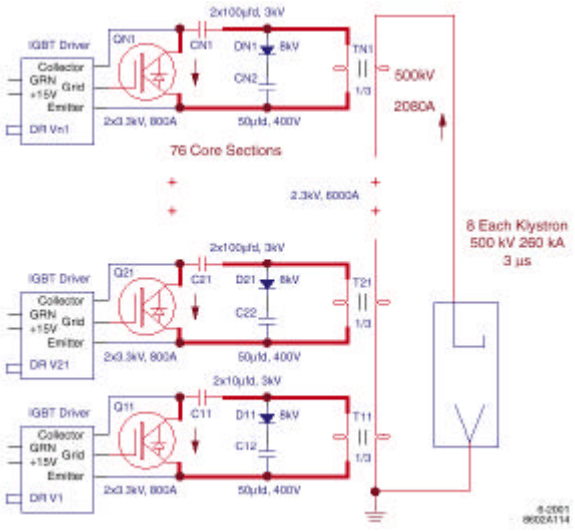

Klystrons:

Klystrons are microwave amplifiers which convert the pulsed dc from the modulators into rf. The principal of operation is straightforward and is schematically illustrated below: a dc beam is generated at a cathode, the non-relativistic beam is velocity modulated at an rf cavity driven by a low power rf signal, the beam bunches as it drifts along the klystron, and rf is extracted from the modulated beam. The output rf power is proportional to the dc beam current and voltage. The beam self-fields are characterized by the perveance: $K = I / V^{3/2}$ and this has a strong effect on the efficiency—smaller perveance is better. The three solutions to this are to use operate at high voltage as is done with the NLC klystrons, use multiple beams as is done in the TESLA klystron or to go to flat (sheet) beams which is being pursued at SLAC. The following table lists the NLC and TESLA klystron parameters.

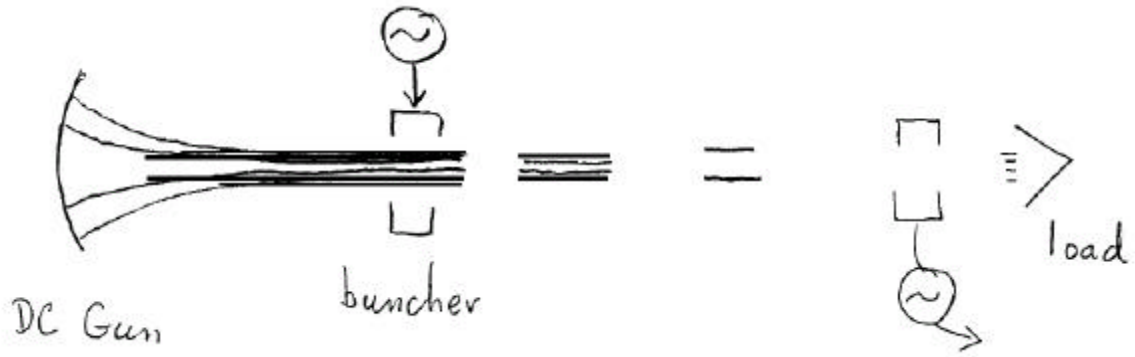

Figure 11: Schematic of a klystron rf amplifier

To couple well to the input and output rf cavities, the beam pipe aperture should be a small fraction of the rf wavelength—this makes high-power high-frequency klystrons more difficult. Another big challenge for all of the high power klystrons is to make sure that the beam loss is minimal. Historically, solenoids have been used to focus the beam as it bunches in the drift tube however recently klystrons have been design using permanent magnets to focus the beams—for the NLC klystrons, the solenoids used a significant amount of power.

Table 2: Parameters of the NLC and TESLA klystrons

	NLC	TESLA
Rf frequency	11.424 GHz	1.3 GHz
Beam Voltage	490 kV	115 kV
Beam Current	260 A	130 A
Rf pulse length	3.2 μs	1.5 ms
Output power	75 MW	10 MW
Input power	1 kW	160 W
Efficiency	60%	65%

RF Pulse Compression and Transport:

The high frequency normal conducting linacs require high peak power in short pulses but klystrons and modulators more naturally produce long pulses of lower peak power → compress the rf power while increasing the peak power. There are many different schemes to compress the rf power: the SLAC Energy Doubler (SLED) which was used for the SLC, SLED-II which is operating on the NLC Test Accelerator, Binary Pulse Compression (BPC), Delay Line Distribution System (DLDS), etc. The basic concept is to make use of 3-dB hybrids (in one form or another) and use variations in the klystron phase to direct the power to different locations. A schematic of a 4x BPC system follows:

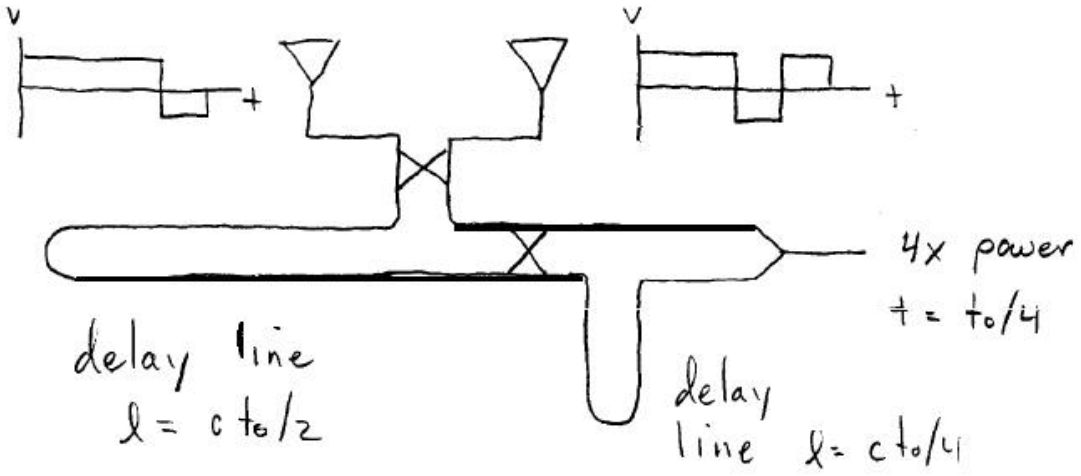

Figure 12: Schematic of BPC rf pulse compression system

Where the crosses represent 3-dB hybrids which direct the rf power to one arm or the other depending on the relative rf phases. The rf voltage from the first klystron is flipped in phase after ¾ of the rf pulse while the rf phase of the klystron is flipped in phase at ½ the rf pulse length and then back again at the ¾ point. This yields 8x the peak power of one klystron (the two klystrons are added together) in ¼ of the rf pulse length.

At high rf frequencies it is important to use low-loss rf modes because the attenuation scales as $f^{3/2}$. For this reason, the TE01 circular mode is used instead of the TE10 rectangular mode which is the mode commonly used to couple to rf cavities. Another variation on the concept is to use multiple modes within the same waveguide to reduce the amount of waveguide that is required.

The DLDS scheme is presently being considered for the NLC. Here, the klystrons phases are used to direct the rf to different groups of accelerator structures. The rf is fed in the direction opposite to that of the beam and the structures are placed so that it takes the beam ½ of the rf pulse length to travel between feeds. In this way, the rf is fed to each group just as the beam arrives. A schematic of a 4x DLDS compression which uses four modes follows—this system is thought to be too complicated to be practical however using 2

different modes does seem reasonable and the current NLC scheme is a dual-moded 8x compression.

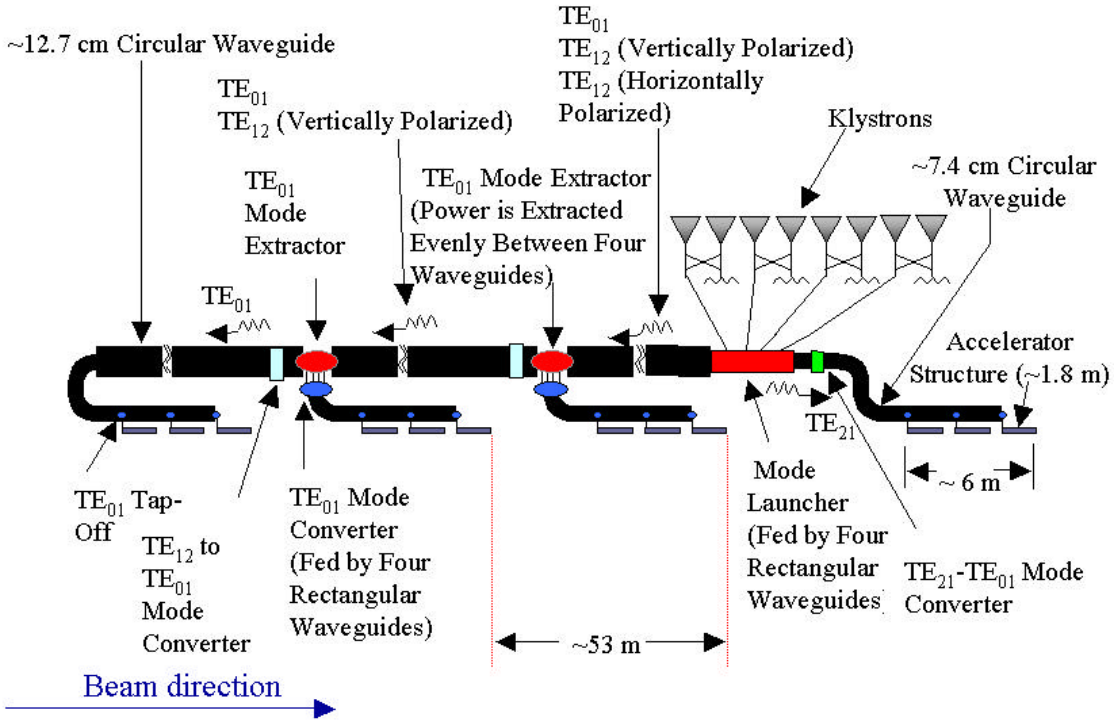

Figure 13: Schematic of a multimoded DLDS 4x compression system

In the superconducting design, the peak power of the rf system is reduced and there is no need for any rf pulse compression. However, the transport from the klystrons to the cavities is still important. In the TESLA design, each klystron feeds 36 cavities. Because the cavities are standing wave cavities, each cavity has a circulator associated with it so that the reflected rf power at the beginning and end of the rf pulse is not reflected back to the klystron. Further, to be able to match the cavities to the beam, each cavity has an adjustable input coupler which feeds slightly more than 200 kW during the rf pulse. The adjustable couplers can be used to change the input power flow for different beam currents. There has been and still is significant development associated with the couplers and less so the circulators.

4. Linear Collider Subsystems

As Steve Holmes discussed, bending a high-energy electron of positron beam will cause substantial synchrotron radiation. This will cause the beam to lose energy and, more importantly, it will dilute the beam emittance. Thus to obtain high luminosity in a linear collider facility, one needs to accelerate high power beams at each other and then focus them to very small spot sizes. The basic layout of the linear collider facilities consists of:

- Electron and positron sources to generate long bunch trains (hopefully polarized)
- Damping rings to decrease the beam emittance
- Bunch compressors to decrease the damping ring bunch length to something matched to the linac
- Efficient main linacs to accelerate the beam to the desired energy without diluting the beam emittance
- Final focus systems to focus the low emittance beams to the small spots sizes needed at the IP

The NLC and TESLA schematics are shown below illustrating the different sections (none of which are drawn to scale although both facilities are roughly the same overall length). In the following, we will discuss each of these regions in a bit more detail.

Polarized Electron Sources:

Linear colliders can collide polarized beams which can aid the analysis greatly. It is relatively easy to generate polarized electrons using a polarized laser and a GaAs photocathode. There are two type of electron guns: dc guns with sub-harmonic bunchers like that used in the SLC and rf guns.

The sub-harmonic bunchers use a high voltage dc gun 100 ~ 200 kV, a photocathode, and a 'long' pulsed laser which generates a beam with a length the order of a nanosecond. This is followed by elements to velocity modulate the long bunch and shorten it. The SLC buncher used cavities operating at 178 MHz and the NLC is designed to use cavities operating at 714 MHz. After drifting a distance and bunching, the beam is captured in a high gradient accelerator section and accelerated to relativistic energies. The problem with the sub-harmonic systems is space charge. Space charge limits the transverse and longitudinal emittances that can be obtained. The NLC system is designed to generate bunches of $2x10^{10}$ with a normalized rms emittance of $\gamma\varepsilon \sim 7x10^{-5}$ in a bunch length of +/-18 ps.

Rf guns avoid the space charge limitations by placing the photocathode in an accelerator cell. A short bunch is generated with short pulsed laser and rapidly accelerated to relativistic

velocities. In principal, rf guns should be able to produce beams with better transverse emittances and smaller bunch lengths. However, typical rf guns operate with very robust photocathodes and it is not clear whether the delicate GaAs cathodes can survive in such an environment which typically has poor vacuum and significant back bombardment of electrons. The SLC polarized dc gun routinely produced polarizations of >78% however it lived in a very clean environment with a vacuum pressure of 10^{-11} Torr and a bending system to prevent decelerated electrons from reaching the photocathode. Another concern regarding the rf guns is the reliability—the SLC e- source had an availability >99%.

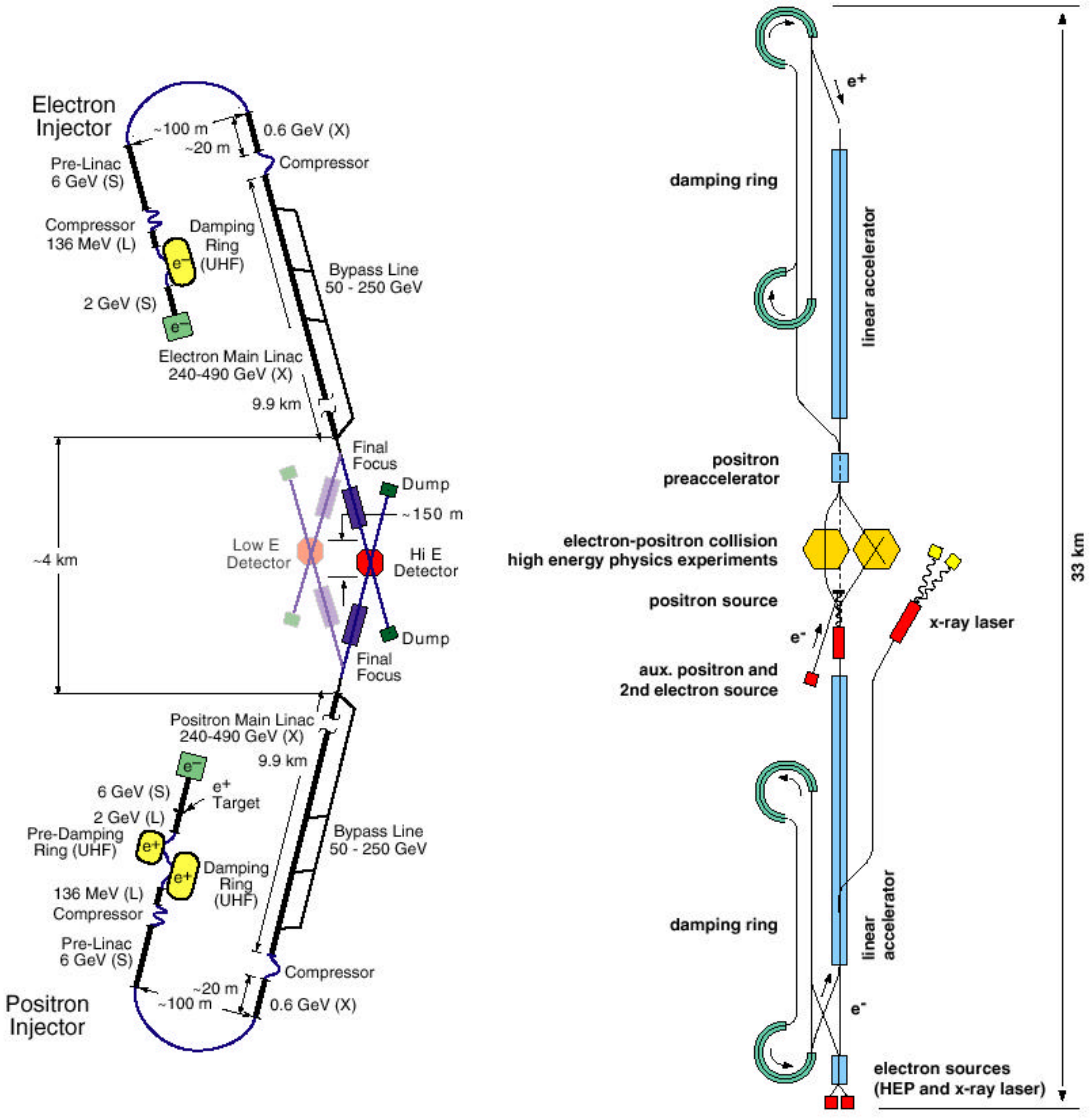

Figure 14: Schematic of the TESLA and NLC linear collider designs

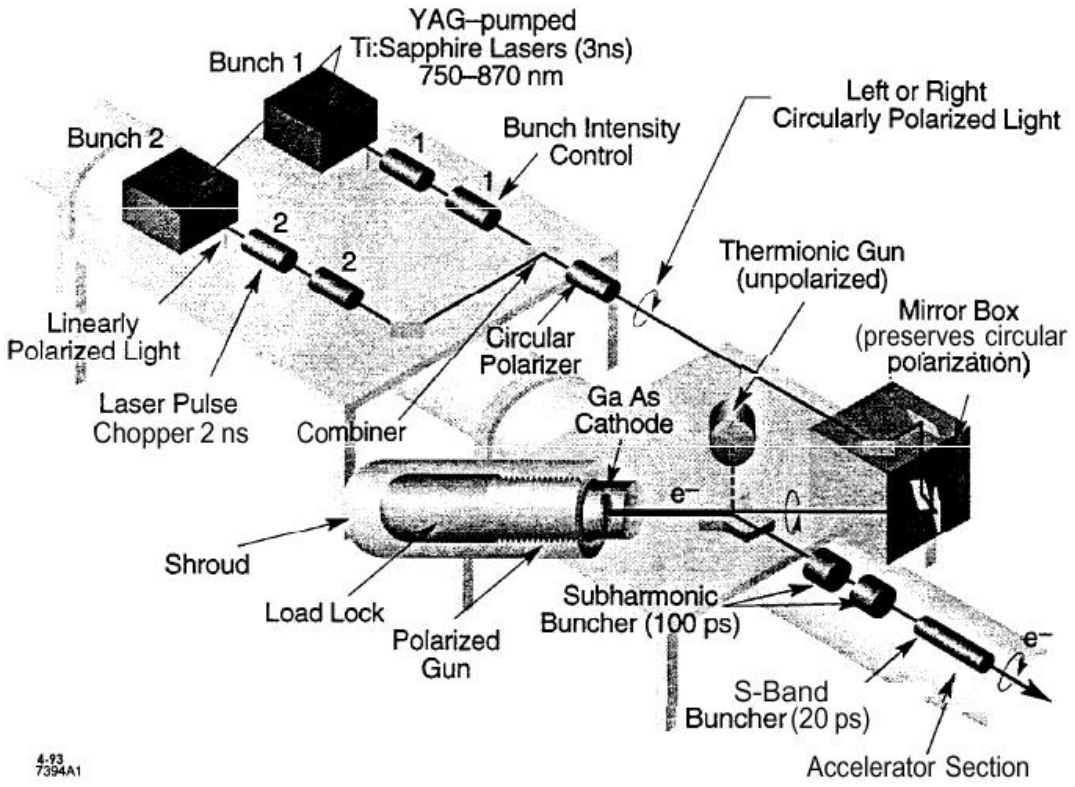

Figure 15: Schematic of the SLC polarized electron source

Positron Sources:

Positrons are captured from an electromagnetic shower. In the SLC, the shower was produced by colliding a 30 GeV electron beam into a WRe target that was roughly 6 r.l. thick. The target must survive both the single pulse heating and the average heating. The average heating is handled by cooling and rotating the target so pulse strike different areas but the single pulse heating must be handled by reducing the cross-sectional density of the incoming electron beam—this forms a limit to the number of positrons that can be produced.

The SLC target failed after 5 years of operation where the typical energy deposition into the target was 50 J/g. This level of energy deposition produces a shock that is roughly a factor of two below the failure level predicted from the ultimate tensile strength of the material however, on examination, it was found that radiation damage had caused the target to become more brittle and thus decrease the failure level.

There are two approaches that are being considered to deal with this problem: (1) simply reduce the energy deposition per target—to generate the desired number of positrons, the

NLC design interleaves the bunch between three targets roughly 4 r.l. thick. (2) adopt a new approach being pursued by the TESLA design where high-energy photons are directed onto the target rather than electrons—this reduces one stage of the shower production and allows the use of a thin target (0.5 r.l.) with a much lower energy deposition. The difficultly with this later approach is that very high-energy photons are needed—the yield is tiny for photon energies below 10 MeV. To produce the photons, the TESLA design passes a high-energy electron beam through a long undulator. The undulator period is 2 cm and the electron beam has to be in excess of 150 GeV. Because of the very high energy that is required, the TESLA design uses the primary (luminosity producing) electron beam.

One advantage of this approach is that, with modifications, it could be used to generate a partially polarized, about 50%, positron beam. Polarized photons are generated using a helical undulator and then polarized positrons are captured by only selecting the high-energy positrons that are produced. The yield in this case is less than 50% of that for the unpolarized capture. Another approach to generating polarized positrons is to use a polarized laser however this requires a very powerful laser system ~ 100 J.

Finally, all of the positron production schemes produce beams with very large phase spaces. Typical normalized emittances from the NLC or TESLA positron source design is $\gamma\varepsilon \sim 0.03$ m-rad. To capture the beams, low frequency rf systems are used and then they must be injected into damping rings which have very large acceptances.

Damping Rings:

The damping ring systems must reduce the relatively large incoming beam emittance to the values desired for luminosity. The challenges for the ring are to damp the beams sufficient fast, generated the very small emittances desired, and have sufficiently large dynamic apertures to capture the incoming beams. The rings also have another purpose. Because the downstream systems are very sensitive to the detailed properties of the beams, the rings provide a relatively long period of time to damp incoming transients and measure the beam properties so feedforward systems can adjust the linac.

As discussed, the average synchrotron radiation in storage rings leads to damping of the phase space while discrete nature of the radiated photons cause an excitation. The equilibrium emittance arises when the two rates are equal. The extracted beam emittance can be written:

$$ge_{ext} = ge_{inj} e^{-2t/t} + ge_0 (1 - e^{-2t/t})$$

where t is the storage time, τ is the radiation damping time, and ε_0 is the equilibrium emittance. To operate as a damping ring, we need small equilibrium emittances and fast damping times. The damping time, divided by the ring revolution period T_0, and the equilibrium emittance can be written:

$$\left(\frac{t_{x,y}}{T_0}\right)^{-1} = 9.4\times10^{-16}\frac{g^3}{J_{x,y}}\oint G^2 ds \qquad G = \frac{1}{?}$$

$$ge_o = 3.84\times10^{-13}\frac{g^3}{J_{x,y}}\frac{\oint G^3 H_{x,y} ds}{\oint G^2 ds} \qquad H = \frac{(1+a^2)}{b}h^2 + 2ahh' + bh'^2$$

Unfortunately, these two quantities scale in the same way, making it difficult to get fast damping and small emittances. In particular, the beam energy cannot be used to attain fast damping because it leads to large emittance—the ring energy is usually chosen to be as low as reasonable to minimize the cost of the rings and is typically a few GeV. The main free parameter is the dispersion invariant *H* which can be made small in a ring with strong focusing or can be made small in a wiggler. The solution pursued in the TESLA damping ring is to use >400 meters of damping wiggler where *H* is very small. The NLC rings use a combination of shorter wigglers (50 meters) and a low emittance arc lattice like that of the synchrotron radiation sources. Both the TESLA and the NLC rings have arcs based on "Theoretical Minimum Emittance" (TME) lattices—these are compact arc cells that have small contributions to the dispersion invariant *H*. The optics of one NLC damping ring cell are shown below.

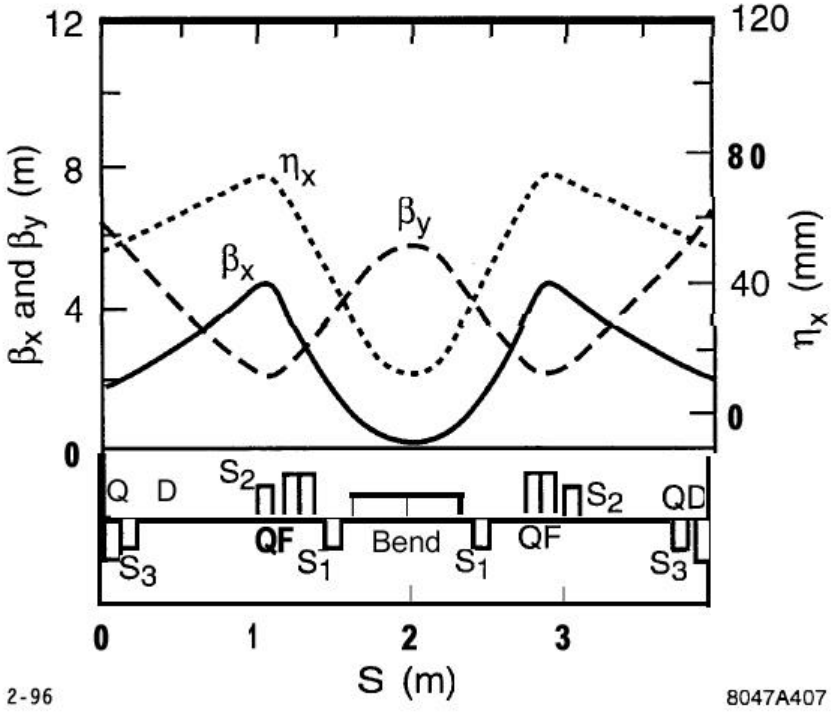

Figure 16: Optics of a TME arc cell

The NLC damping ring is designed to operate at 1.98 GeV and is roughly 300 meters in circumference and stores three trains of bunches at once. Each bunch train is injected and

extracted on a rf pulse with a kicker—the bunch trains are separated by 65 ns to allow for the kicker rise and fall times. This means that each bunch train is stored for 3 * 1/120 Hz ~ 25 ms during which period the beam emittance must be damped to the desired values.

The TESLA damping ring has a different problem. Because bunches in TESLA are spaced far apart, storing the uncompressed TESLA bunch train would require a circumference of ~300 km. Instead, the bunches are injected and extracted individually with a very fast kicker—the design calls for a bunch spacing of 25 ns for the 500 GeV cms parameters and 11 ns at 800 GeV cms. Even with this compression, the ring has to be roughly 17 km in circumference. In this case, all of the bunches are stored for one intrapulse period of 1/5 Hz = 200 ms. The beam energy is designed to be 5 GeV.

Both damping rings are designed to produce very small beam emittances—much smaller than those produced in typical synchrotron radiation sources. This leads to a number of issues: first, the alignment tolerances in the rings tend to be tight ~ 50 mm; second, the beam density is very high meaning that the space charge depression, intrabeam scattering and Touschek lifetimes are all significant issues; third, because of the sensitivity of the downstream systems, the damping rings cannot operate with transient effects that will cause variations in the extracted beam—most d.c. effects can be treated by optimizing the downstream systems—this means that the rings are very sensitive to collective instabilities; finally, because the injected beam emittances are relatively large, the rings must have large dynamic apertures so that the injection losses are small.

Another issue for the damping rings is that they must preserve the polarization of the injected beams. This requires rotating the polarization vector to a vertical orientation before injection into the ring. To avoid spin-orbit imperfection resonances, it is important to choose the energy to keep the spin tune far from an integer: $\nu_{spin} = E/440$ MeV. The energy of the NLC ring is chosen to operate with a spin tune close to the ½ integer. This is based on experience with the PEP, SPEAR, and SLC storage rings—a plot of the polarization versus spin tune is shown below for the SLC damping ring which had a nominal operating energy of 1.2 GeV or $\nu_{spin} = 2.7$ and was unfortunately close to a depolarizing resonance at $\nu_{spin} = 2.75$.

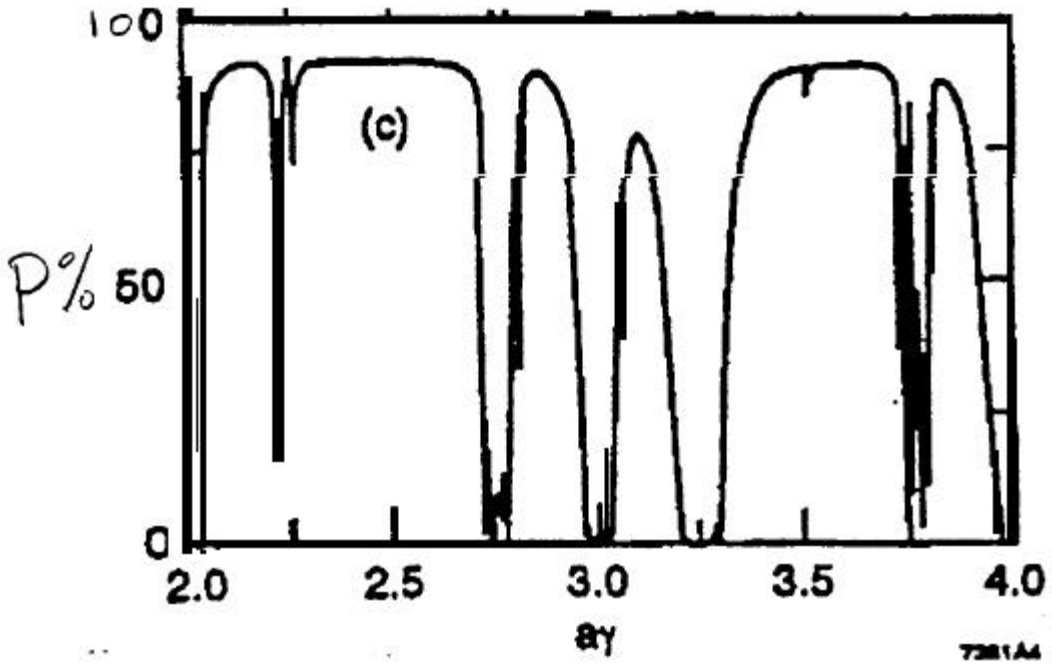

Figure 17: Calculation of polarization versus spin tune in SLC damping ring

Bunch Compressors:

The damping rings produce beams that are roughly 5 mm in length. The bunches are then shortened for three reasons: (1) to prevent large energy spread in the linac due to the curvature of the rf; (2) to reduce the tranverse wakefield emittance dilutions, the bunch is compressed after the damping rings; (3) to reduce the disruption parameter. The typical bunch lengths are 300 μm in TESLA and 100 μm in NLC.

Magnetic bunch compressors operate by adding a correlated energy deviation along the bunch length and then passing the beam through a region where the path length is energy dependent—this is generated using bending magnets to create dispersive regions. The first-order path length dependence is:

$$\frac{dz}{dd} = R_{56} = \int hGds$$

while the energy-position correlation from an rf section is:

$$\frac{dd}{dz} = R_{65} = \frac{V_{rf} k_{rf} \sin(f_{rf})}{E_0 + V_{rf} \cos(f_{rf})}$$

where E_0 is the initial beam energy and Vrf, κrf and ϕrf are the rf voltage and wavenumber and phase—for greatest effect, the beam is placed at the zero-crossing on the rf wave.

The rf sections and dispersive regions operate on the longitudinal phase space in a manner analogous to the way quadrupole and drifts effect the transverse phase space. The simplest compressor design is one composed of a single rf section followed by a dispersive region—this performs an approximate 90 degree rotation of the longitudinal phase space. When tuned for maximum compression, the resulting bunch length is roughly:

$$\sigma_{z,final} \approx R_{56}\sigma_{E,initial} \qquad \sigma_{E,final} \approx \sigma_{E,initial}\frac{\sigma_{z,initial}}{\sigma_{z,final}}$$

In the NLC, two-stages of bunch compression are used to attain the 100 μm lengths desired. The first stage is a 90 degree rotation performed immediately after the damping ring and the second stage is a 360 degree rotation performed at an energy of 8 GeV after in energy spread has been reduced again after acceleration—a schematic of the NLC compressor scheme follows. This two-stage procedure is used to: (1) limit the maximum energy spread in the beam at any time which limits chromatic errors as well as reduces the effect of nonlinearities in the compressor itself, (2) reduce the coherent synchrotron radiation that is produced, and (3) perform a net 90 degree rotation between the damping ring and the IP so that phase errors in the damping ring beam do not become energy errors at the IP.

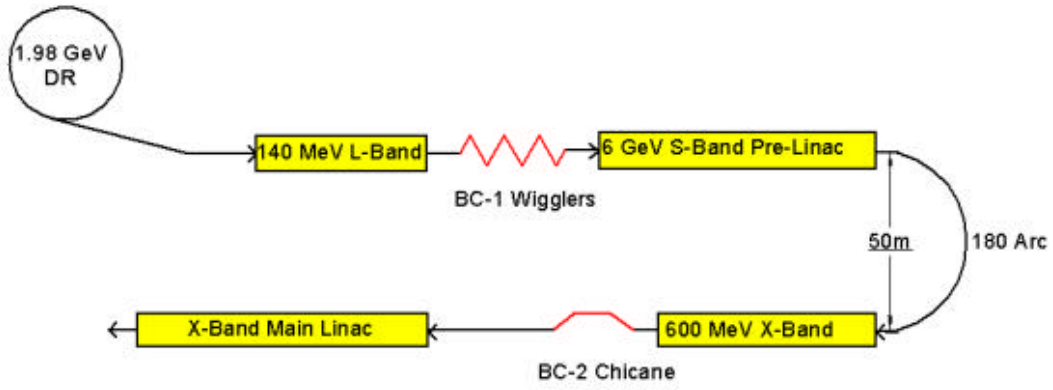

Figure 18: Schematic of the NLC two-stage bunch compressor system

Linac Optics and Emittance Dilutions:

The main linacs have to accelerate the beams to very high energy while preserving the beam transverse and longitudinal emittance. The linacs are usually designed as a simple FODO lattice that is scaled so that the beta functions and cell lengths increase with the beam energy. The advantages of the regular FODO lattice is that it is easy to tune and match and the periodicity makes the lattice relatively insensitive to energy errors—this reduces the chromatic filamentation and mismatches that arise with energy variation in the beam. The strength of the focusing lattice is a balance between reducing the wakefield effects with strong focusing and easing the dispersive and jitter tolerances with weak focusing.

The primary sources of emittance dilution are usually separated into those that affect the bunch train and those that impact a single bunch. The long-range effects are really just the long-range longitudinal and transverse wakefields while the single bunch dilutions include the short-range wakefields but also include betatron coupling, dispersive errors, rf deflections, and ground motion and jitter effects. Because the vertical beam emittance is much less than the horizontal, all of these effects are more important in the vertical.

All of these sources of dilution are 'conservative' forces and thus they cannot really dilute the phase space density. Instead, they couple the transverse and longitudinal degrees of freedom increasing the projection of the beam at the IP. For example, a transverse wakefield will deflect the tail of the beam onto a trajectory different from the head of the beam. At the IP, this looks like the beam size has been increased. Unfortunately, it is the projection that determines the luminosity and thus these effects are important.

The beam has a 6-D phase space volume (x, px, y, py, z, δE). The dilutions cause:

- Transverse wakefields: (z → y)
- Disperive errors: (dE → y)
- Rf deflections: (z → y)
- Betatron coupling: (x, px → y)
- Jitter: (t → y)

The projected rms emittance is given by:

$$e^2 = < (x - \bar{x})^2 >< (x' - \bar{x'})^2 > - < (x - \bar{x})(x' - \bar{x'}) >^2$$

where the angle brackets and the overbars both denote ensemble averages over the particle distribution.

In addition, there are a few non-conservative forces that can be important if ignored. These include beam-gas scattering, where individual particles scatter off residual gas atoms, synchrotron radiation, where individual particles emit photons and change there trajectory,

and intra-beam scattering, where individual particles within a beam scatter off of each other. With a reasonable design, these effects can be made small and we will not discuss them.

The long-range longitudinal wakefield is really just the beam loading, i.e. the energy extraction from the rf cavity, that was discussed in connection with the rf-to-beam efficiency. In both NLC and TESLA, the effect of the long-range wakefield is compensated by varying the rf fields in the cavity as the beam passes.

The long-range tranverse wakefield is directly controlled by careful design of the accelerator structures and can be made relatively unimportant in both the TESLA and NLC designs.

In the following, we will briefly discuss the emittance dilution due to the short-range transverse wakefield from misaligned accelerator structures. As an aside, the transverse wakefield is due to higher-order modes in the cavities. The lowest deflecting mode is a TM_{11}-like mode where the longitudinal electric field has a J_1 Bessel function radial dependence—thus it is zero on axis and grows linearly for small deviations from the axis. This couples to a beam that is off-axis in the cavity. The transverse magnetic field which actually causes the deflection lags by $\pi/2$.

All of the details of the cavity modes are described in terms of the 'wakefield': $W_\perp$. Thus, the equation of motion can be written:

$$\frac{d^2 y(z)}{ds^2} + (1-d)K_1 y(z) = \frac{Nr_0}{g}\int_z^\infty dz' r(z') y(z') W_\perp(z'-z)$$

where K is the normalized quadrupole strength, ρ is the longitudinal distribution function, and $\delta = \Delta E/E$. For a two-particle model, where the beam is represented by two particles with charge $N/2$ located at + and $-\sigma z$, this reduces to Eq. 2-58 in Kwang-Je Kim's notes where he discussed the Beam Breakup (BBU) instability and the correct using BNS damping.

To estimate the emittance dilution due to randomly misaligned structures, we first, consider the effect of a single misaligned accelerator structure with a length Lacc and an offset yacc. Assuming that the wakefield is weak and the structure short compared to the betatron wavelength, it can be represented as a single deflection:

$$\Delta y'(z) = L_{acc}\frac{Nr_0}{g} y_{acc}\int_z^\infty dz' r(z') W_\perp(z'-z)$$

In the two-particle model this simplifies to $\Delta y'_2 = L_{acc}\, y_{acc}\, N\, r_0\, W(2\sigma_z)/(2\gamma)$ and the leading particle is unaffected.

To calculate the increase in the projected phase space area, i.e. the effective emittance growth, we have to sum these deflections and subtract off the centroid motion.

In this two-particle model, the rms increase in $\Delta y'$ is ½ of the kick given to the tail particle. If this is put into the expression for the emittance, and it is assumed that the dilution is small, the emittance increase can be written: $\Delta\varepsilon = \beta\, \Delta y'^2/2$.

Finally, we need to sum the effects of many different structures randomly misaligned. If we ignore the beam acceleration and the change in the beta-functions along the accelerator, the emittance growth is just multiplied by the number of misaligned structures. A more exact result can be found by including these slowly varying functions but the above approximation gives the correct order-of-magnitude.

Final Focus Systems:

The final focus must demagnify the beams to the very small spots sizes required for the luminosity. Because the quadrupole focusing is naturally asymmetric (focusing in one plane while defocusing in the other), this is done using a strong final lens which is constructed from a doublet of quadrupoles for asymmetric collisions or a quadrupole triplet for equal IP beta functions. The magnets are located a distance L* from the IP – L* cannot be too small because of the finite quadrupole strengths and the need to have free space around the IP for the detector -- typical values of L* are a few meters.

The beam sizes are given by: $\sigma=\mathrm{sqrt}(\beta\varepsilon)$. In the field-free region between the IP and the final magnets, the beta functions evolve as:

$$b(s) = b^* + s^2 / b^*$$

where β^* is the beta function at the IP.

The strong focusing is very sensitive to the energy spread in the beam. Typical beam energy spreads are $\Delta E/E \sim 10^{-3}$. Small variations in the focusing due to the energy deviation will cause changes in the waist location and thereby increase the spot size at the IP as illustrated below.

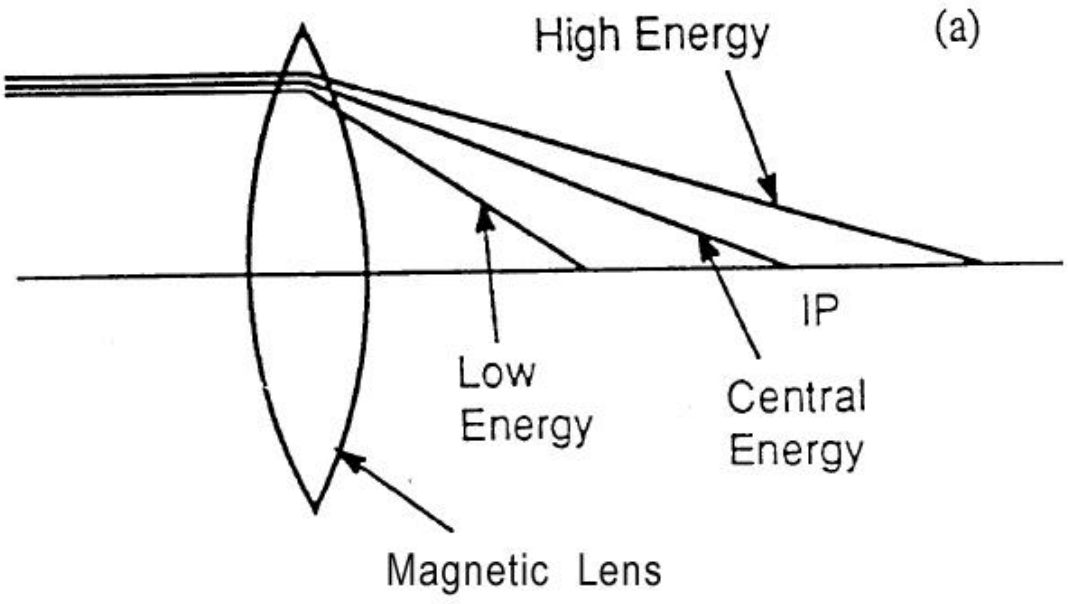

Figure 19: Schematic of the effect of the chromatcity on the IP spot size

From geometric considerations, the variation in the spot size is roughly:

$$\frac{\Delta s}{s} \approx \frac{L^*}{b^*} s_{\Delta E/E}$$

This variation in the waist location is referred to the chromaticity ξ. The value of the chromaticity in NLC is roughly 30,000 and thus a typical energy spread of 3×10^{-3} will increase the IP spot size by 100 times.

To correct the chromaticity, need to add (subtract) focusing for high (low) energy particles. This can be done using sextupole magnets in regions of dispersion where the particle position has a linear correlation with the beam energy deviation. The pole configuration for quadrupole and sextupole magnets is shown below:

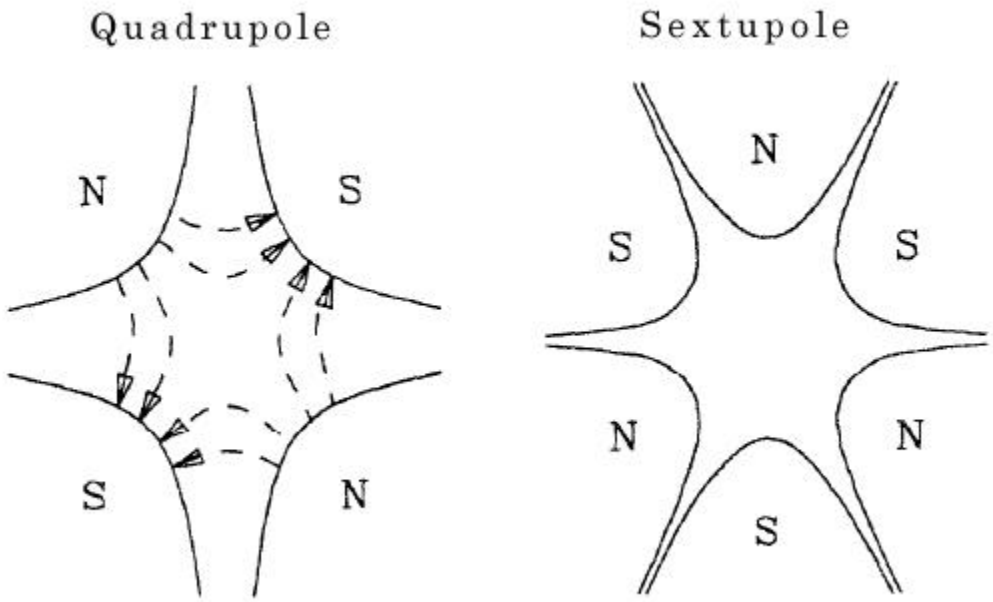

The vertical field in a quadrupole magnet with an aperture a is: $By(x,y) = x\ Bpole/a$ while the field in a sextupole is: $By(x,y)=(x^2-y^2)\ Bpole/a^2$. If the sextupole is placed in a region of disperion, where $x = x_\beta + \eta\ \Delta E/E$, then the sextupole generates an energy dependent focusing as well as an unwanted nonlinear aberration from the x_β^2 and the y^2 terms. To correct the effect of the final focusing magnet the sextupole must be placed an integral number of half betatron wavelengths away, i.e. $n\pi$ upstream of the final magnet.

To cancel the nonlinear aberrations that the sextupoles introduce, a pair of sextupoles are used which are placed 180 degrees in betatron phase apart. An example of such a scheme is shown below—in this case, the final sextupoles are placed at the final focusing magnet location and a non-zero dispersion is generated in the final magnets with a bending magnet just upstream. This approach therefore corrects the chromaticity of the final magnets locally which is can yield very good performance however the linear dispersion and higher-order terms must be corrected to zero at the IP. To correct the sextupole aberrations, another pair of sextupoles is placed 180 degrees in betatron phase upstream of the pair performing the chromatic correction.

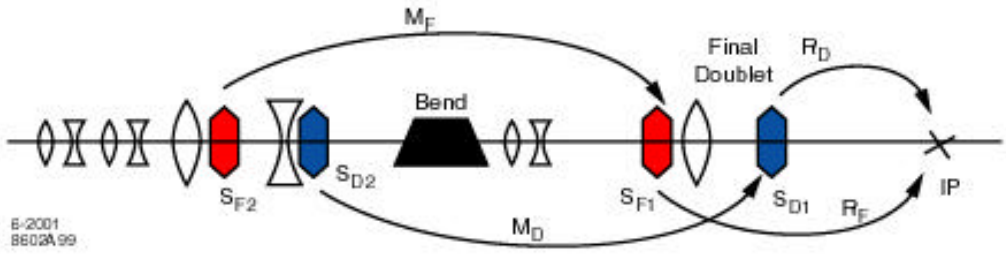

Figure 20: Schematic of new NLC final focus with local chromatic correction

This local correction concept for a final focus is quite recent and has not been demonstrated experimentally. The Final Focus Test Beam at SLAC was based on a system where the chromatic correction of the two planes was not interleaved and was performed in dedicated chromatic correction sections. A schematic of the FFTB is shown below—this disadvantage of this approach is that the system requires additional bending, which at high energy, has to be very weak to prevent synchrotron radiation induced emittance growth and thus makes the final focus very long.

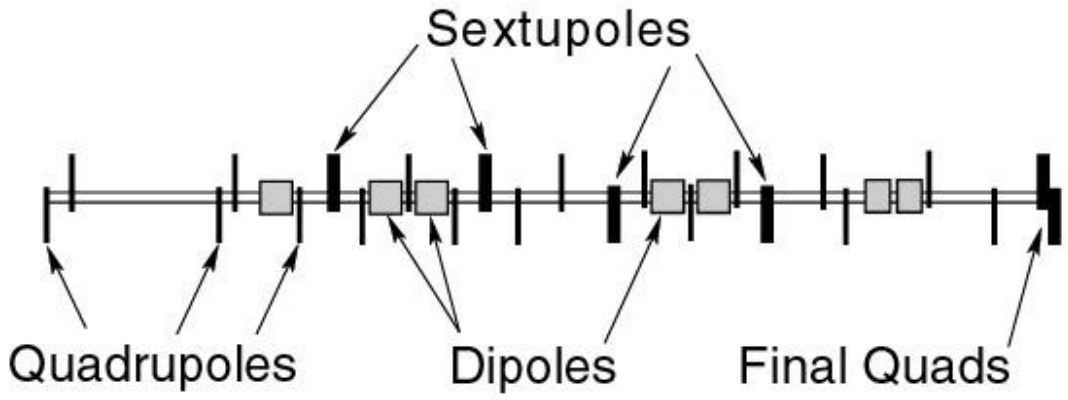

Figure 21: Final Focus Test Beam beam line

The remaining 4th-order aberrations can be corrected with additional nonlinear elements including sextupoles, octupoles, and higher-order multipoles.

Table 1.1 Overall Parameters

	TESLA		JLC (C)		JLC/NLC* (X)		CLIC	
Center of mass energy	500 GeV	800 GeV	500 GeV	1000 GeV	500 GeV	1000 GeV	500 GeV	3000 GeV
RF frequency of main linac (GHz)	1.3		5.7		11.4		30	
Peak luminosity (10^{33}cm^{-2}s^{-1})	34	58	7.95	8.41	25.0 (20.0)	25.0 (30.0)	14.2	103
Linac repetition rate (Hz)	5	4	100		150 (120)	100 (120)	200	100
No. of particles/bunch at IP (10^{10})	2	1.4	1.1	1.4	0.75		0.4	
No. of bunches/pulse	2820	4886	72		192		154	
Bunch separation (nsec)	337	176	2.8		1.4		0.67	
Beam power/beam (MW)	11.3	17	3.2	4.0	8.6 (6.9)	11.5 (13.8)	4.9	14.8
Unloaded/loaded gradient† (MV/m)	23.4 / 23.4	35 / 35	42 / 33.9	59.5 / 49.2	70 / 55		172 / 150	
Total two-linac length (km)	30	30	17.7	24.9	12.6	25.8	5.0	27.5
Total beam delivery length (km)	3		XX		3.7		7	
Proposed site length (km)	33		XX		32		40	
Tunnel configuration	Single		Double		Double		Single	

* Numbers in ( ) correspond to US site with 120 Hz repetition rate.

† The main linac loaded gradient includes the effect of single-bunch (all modes) and multibunch beam loading, assuming that the bunches ride on crest. Beam loading is based on bunch charges in the linacs, which are slightly higher than at the IP.

Table 1.2 Damping Rings

	TESLA		JLC (C)		JLC/NLC* (X)		CLIC	
	500 GeV	800 GeV	500 GeV	1000 GeV	500 GeV	1000 GeV	500 GeV	3000 GeV
Damping Ring Systems								
Damping ring complex energy (GeV)	5				1.98		1.98	4.6
Number of rings in complex	2				3		3	3
No. of bunches/train	2820	4886			192		154	
No. of particles/bunch (10^{10})	2	1.4			0.8		0.42	
Bunch spacing (ns)	20	11.5			1.4		0.66	
Injected beam emit.† $!^2_{e+}$ / $!^2_{e!}$ [mm-mrad]	10,000 / 10				45,000 / 150		10	
Extr. beam emit.† $!"_x$ / $!"_y$ [mm-mrad]	8 / 0.02	6 / 0.01			2.2 / 0.02		1.6 / 0.003	0.5 / 0.003
Positron (Pre-)Damping Rings‡								
Ring circumference (m)	17,000				231		307	2600
Number of trains stored	1				2		8	XX
RF frequency & voltage (MHz/MV)	500 / 54				714 / 1.5		1499	XX
Wiggler length [m]	432				50		40	XX
Damping times ($\#_x$/$\#_y$/$\#_z$) (ms)	28 / 28 / 14				5.8 / 5.8 / 2.9		XX	XX
Tunes ($\$_x$/$\$_y$/$\$_z$)	72.28 / 44.18 / 0.1				11.465 / 5.388 / 0.0114		XX	XX
Bunch len. $\%_z$ & energy spr. $\frac{!_E}{E}$ (mm / %)	6 / 0.13				5.1 / 0.08		3 / 0.08	3 / 0.08
Equil. beam emit. $!"_x$ / $!"_y$ [mm-mrad]	8 / 0.02	8 / 0.01			60 / 60		1600 / XX	XX
Electron Damping Ring‡								
Ring circumference (m)	17,000				300		307	
Number of trains stored	1				3		8	
RF frequency & voltage (MHz/MV)	500 / 30				714 / 1.1		1499	
Wiggler length [m]	250				46		40	
Damping times ($\#_x$/$\#_y$/$\#_z$) (ms)	50 / 50 / 25				4.8 / 5.1 / 2.6		XX	
Tunes ($\$_x$/$\$_y$/$\$_z$)	72.28 / 44.18 / 0.1				27.26 / 11.13 / 0.0035		XX	
Bunch len. $\%_z$ & energy spr. $\frac{!_E}{E}$ (mm / %)	6 / 0.1				3.6 / 0.09		3 / 0.08	
Equil. beam emit. $!"_x$ / $!"_y$ [mm-mrad]	8 / 0.02	6 / 0.01			2.2 / 0.01		1600 / XX	

* Numbers in table correspond to NLC damping ring designs with 120 Hz repetition rate.

† Injected emittances are assumed round but different for e^+ and e^- while extracted emittances are equal for e^+ and e^- but asymmetric

‡ Positron Ring table describes TESLA e+ ring and NLC/JLC/CLIC positron pre-damping rings while Electron Ring table describes TESLA e- ring and NLC/JLC/CLIC electron and positron main damping rings.

Table 1.3 Pre-Linacs and Bunch Compressors

	TESLA		JLC (C)		JLC/NLC* (X)		CLIC	
	500 GeV	800 GeV	500 GeV	1000 GeV	500 GeV	1000 GeV	500 GeV	3000 GeV
Electron booster linac (e! source " damping rings)								
Initial and Pnal energy (GeV)	0.5 / 5				0.08 / 1.98		0.2 / 2	0.2 / 4.6
RF frequency (GHz)	1.3				2.8		1.5	
Unloaded and loaded gradient† (MV/m)	20 / 20				19.3 / 16.2		21 / 17	
Total length (m)	305				164		120	300
Positron booster linac (e+ source " damping rings)								
Initial and Pnal energy (GeV)	0.3 / 5				0.25 / 1.98		0.2 / 2	0.2 / 4.6
RF frequency (GHz)	1.3				1.4		1.5	
Unloaded and loaded gradient† (MV/m)	20 / 20				14.1 / 12.5		21 / 17	
Total length (m)	400				164		120	300
First stage bunch compressor								
Initial and Pnal bunch length (mm)	6 / 0.3				4 / 0.5		3 / 0.25	XX
Initial and Pnal energy spread (%)	0.13 / 2.7				0.09 / 1.0		0.08 / 1.0	XX
RF frequency (GHz)	1.3				1.4		3	XX
RF voltage (MV)	890				139		103	XX
Total length (m)	400				51		35	XX
Pre-linac (damping rings " 2nd bunch compressor)								
Initial and Pnal energy (GeV)	Not needed				1.98 / 8		2 / 9	4.6 / 9
RF frequency (GHz)					2.8		3	
Unloaded and loaded gradient† (MV/m)					19.3 / 16.8		21 / 17	
Total length (m)					485		415	260
Second stage bunch compressor								
Initial and Pnal bunch length (mm)	Not needed				0.5 / 0.1		0.25 / 0.03	XX
Initial and Pnal energy spread (%)					0.25 / 1.5		0.22 / 1.8	XX
RF frequency (GHz)					11.4		30	
RF voltage (MV)					583		1026	XX
Total length (m)					212		80	XX

*Numbers in table correspond to NLC design with a 120 Hz repetition rate.

†The linac loaded gradient includes the e! ect of single-bunch (all modes) and multibunch beam loading, assuming that the bunches ride on crest. Beam loading is based on bunch charges in the linacs, which are slightly higher than at the IP.

Table 1.4 Main Linac Parameters

	TESLA		JLC (C)		JLC/NLC* (X)		CLIC	
	500 GeV	800 GeV	500 GeV	1000 GeV	500 GeV	1000 GeV	500 GeV	3000 GeV
Initial Energy (GeV)	5		10		8		9	
RF frequency (GHz)	1.3		5.7		11.4		30	
Unloaded/loaded† gradient (MV/m)	23.4 / 23.4	35 / 35	44 / 34	59.5 / 49.2	70 / 55		172 / 150	
Overhead for fdbk & repair (%)	2		0	0	5		13	10
Overhead for off-crest operation (%)	0.4		0	0	5		XX	XX
Active two-linac length (km)	21.6	23	14.2	19.9	10.1	20.2	3.7	21.5
Total two-linac length (km)	30	30	17.7	24.9	12.6	25.8	5.0	27.5
Total number of klystrons	572	1212	3956	5562	3744 (1872)	7488 (3744)	332	364
Total number of modulators	572	1212	3956	5562	468 (234)	936 (468)	332	364
Klystron peak power (MW)	9.7		50	100	75		50	
Klystron repetition rate (Hz)	5	4	100	50	150 (120)	100 (120)	200	100
Klystron pulse length (μsec)	1370		2.5		1.6 (3.2)		18	100
Pulse compression ratio	1		5		4 (8)		32x4	32x22
Pulse compression gain	1		3.6		3.4 (6.8)		32x4	32x22
RF pulse length at linac (μsec)	1370		0.49		0.40		.13	.13
Number of sections	20592	21816	7912	11124	11232	22464	14544	42940
Section length (m)	1.04		1.8		0.9		0.5	0.5
a/λ (range if applicable)	0.15		0.165—0.130		0.210—0.148		0.212—0.199	
v_g/c (%)	—		3.1—1.3		5.1—1.1		10.4—5.2	
Filling time (ns)	4.2×10^5		296		120		30	
Q Unloaded	10^{10}		10036		9055—8093		3628—3621	
Shunt impedance (MΩ/m)	10^{13}		54.1		81.2		XX	
Total AC power for linacs‡ (MW)	95	160	145	146	150 (120)	200 (240)	100	300
Wall plug to RF efficiency (%)	37.3		24.1	33.8	37.4		40.3	
RF to beam efficiency (%)	62.4	56.5	17.6	15.9	26.7		21.3	

* Numbers in ( ) correspond to US site with 120 Hz repetition rate.

† The main linac loaded gradient includes the effect of single-bunch (all modes) and multibunch beam loading, assuming that the bunches ride on crest. Beam loading is based on bunch charges in the linacs, which are slightly higher than at the IP.

‡ Total AC power includes power for the cryo-plant in a superconducting facility and it includes power for cooling water in a normal conducting facility. It does not include power for distribution and it does not include power for magnets, movers, instrumentation or lighting.

Table 1.5 Linear Colliders: Beam Delivery System and Interaction Point Parameters

	TESLA		JLC (C)		JLC/NLC* (X)		CLIC	
	500 GeV	800 GeV	500 GeV	1000 GeV	500 GeV	1000 GeV	500 GeV	3000 GeV
Beam delivery system length† (km)	3.2		XX	XX	3.8		7.0	
Collimation system length† (km)	1.4		XX	XX	1.4		5.9	
Final Focus system length† (km)	1.2		XX	XX	1.6		1.1	
$\gamma\varepsilon_x / \gamma\varepsilon_y$ (m-rad $\times 10^{-6}$)	10 / 0.03	8 / 0.02	3.6 / 0.05		3.6 / 0.04		2.0 / 0.02	0.68 / 0.02
β_x^* / β_y^* (mm)	15 / 0.4	15 / 0.4	15 / 0.2	30 / 0.2	8 / 0.11	13 / 0.11	10 / 0.15	8 / 0.15
σ_x^* / σ_y^* (nm) before pinch	553 / 5	391 / 2.8	330 / 4.5		243 / 3.0	219 / 2.3	200 / 2.5	43 / 1.0
σ_z^* (μm)	300		200		110		30	
Distance between IP and last quad	3		XX		3.8		4.3	
Crossing Angle at IP (mrad)	0		7		6 (20)		20	
Disruptions D_x / D_y	0.2 / 25	0.2 / 27	0.23 / 16.8	0.14 / 14.9	0.16 / 12.9	0.08 / 10.0	0.12 / 7.9	0.03 / 2.7
H_D	2.1	2.1	1.69	1.62	1.52	1.47	XX	XX
δ_0	0.02	0.21	0.08	0.20	0.14	.29	0.3	8.1
δ_B (%)	3.2	4.8	3.8	7.9	5.4	8.9	4.7	31
n_γ (no. of γs per e)	2.0	1.5	1.46	1.70	1.3	1.3	0.7	2.3
$N_{pairs}(p_T^{min} = 20 MeV/C, \theta_{min} = 0.15)$								
$N_{hadrons}$/ crossing								
$N_{jets} \times 10^{-2} (p_T^{min} = 3.2 GeV/C$								
Nominal Luminosity ($10^{33} cm^{-2} s^{-1}$)‡	16.2	27.9	4.7	5.2	15.2 (12.2)	15.7 (18.9)	XX	XX
Luminosity ($10^{33} cm^{-2} s^{-1}$)‡	34	58	7.9	8.4	25 (20)	25 (30)	14.2	103
$L_{100\%}$ [%]							XX	XX
$L_{99\%}$ [%]							8.17	25.5
$L_{95\%}$ [%]							11.95	40.8
$L_{90\%}$ [%]							13.0	49.0

* Numbers in ( ) correspond to US site with 120 Hz repetition rate.

† System length includes both incoming beamlines

‡ For the sake of uniformity, the nominal luminosity is simply defined as $N^2/4\pi\sigma_x^*\sigma_y^*$ times the number of crossings per second, and in all cases assumes head-on collisions, no hour-glass effect and no pinch. The actual luminosity incorporates all these effects, including crossing angle where applicable plus any additional IP dilutions that may be expected.

Table 1.6 Linear Colliders: Electron and Positron Sources

	TESLA		JLC (C)		JLC/NLC* (X)		CLIC*	
	500 GeV	800 GeV	500 GeV	1000 GeV	500 GeV	1000 GeV	500 GeV	3000 GeV
Repetition Rate (Hz)	5	4			150 (120)	100 (120)	200	100
No. of bunches/train	2820	4886			192		154	
Bunch spacing (ns)	337	176			1.4		0.67	
Electron Source								
Style	Sub-harm. buncher				Sub-harm. buncher		Sub-harm. buncher	
E! beam energy† (GeV)	0.5				0.08		0.2	
No. particles/bunch (10^{10})	4				0.8		0.625	
Polarization (%)	80				80		XX	
Emittance (rms) !"$_x$ / !"$_y$ [mm-mrad]	40 / 40				100 / 100		4 " 7	
Bunch length ! z_{FWHM} (mm)	8				10		XX	
Bunch energy spread ! E/E_{FWHM} (%)	1				2		1 " 2	
Positron Source								
Style	Undulator				Conv. target		Sub-harm. buncher	
E+ beam energy† (GeV)	0.300				0.250		0.2	
No. particles/bunch (10^{10})	2				0.8		0.8	
Polarization (%)	45 " 50				0		0	
Emittance (edge) !"$_x$ / !"$_y$ [mm-mrad]	40,000				30,000 / 30,000		60,000	
Bunch length ! z_{FWHM} (mm)	5				15		XX	
Bunch energy spread ! E/E_{FWHM} (%)	7				15		XX	
Incident beam energy (GeV)	250 —150				6.2		2	
Target material / thickness (r.l.)	Ti / 0.4				WRe / 4		WRe / 4.5	
Number of targets	1				3		XX	
Incident beam spot size (mm)	0.7				1.6		XX	
Yield at damping ring‡ (e+ / e!)	2 at 500GeV / 1 at 300GeV				1		0.59	

* Numbers in ( ) correspond to US site with 120 Hz repetition rate.

† Beam energy is given at the end of the injector system.

‡ Yield is evaluated as number of captured e+ at the system exit or in the damping ring versus number of incident e! .